AIMS Mathematics, 8(3): 5950–5979.
DOI: 10.3934/math.2023300
Received: 08 July 2022
Revised: 21 October 2022
Accepted: 24 October 2022
Published: 27 December 2022

http://www.aimspress.com/journal/Math

Research article

Linear regression of triple diffusive and dual slip flow using Lie Group transformation with and without hydro-magnetic flow

T. Mahesh Kumar[1,†], Nehad Ali Shah[2,†], V. Nagendramma[3], P. Durgaprasad[4], Narsu Sivakumar[5], B. Madhusudhana Rao[6], C. S. K. Raju[7] and Se-Jin Yook[7,*]

[1] Department of Mathematics, Sri Venkateswara University, Tirupati, India-517502
[2] Department of Mechanical Engineering, Sejong University, Seoul 05006, Republic of Korea
[3] Department of Mathematics, Presidency University, Bangalore, Karnataka-India
[4] Division of Mathematics, SAS, Vellore Institute of Technology, Chennai Campus, Tamil Nadu, India
[5] Department of Mathematics, SRM IST-Kattankuluthur, Tamil Nadu, India- 603203
[6] Faculty Mathematics, Department of Information Technology, University of Technology and Applied Sciences, Muscat, Oman
[7] School of Mechanical Engineering, Hanyang University, 222 Wangsimni-ro, Seongdong-gu, Seoul, 04763, Republic of Korea (CSKR)

* **Correspondence:** Email: ysjnuri@hanyang.ac.kr.

† These authors contributed equally to this work and are co-first authors

Abstract: This study examines the flow of an incompressible flow over a linear stretching surface with the inclusion of momentum and thermal slip conditions. A scaling set of alterations is applied to the governing system for both with and without magnetic field situations. The physical system being leftover invariant caused by some associations surrounded by the transformations. Later we find the absolute invariants 3rd -order ODEs for the linear momentum equation and two 2nd order ODEs consistent with the energy and concentration are obtained. The equations that coincide with the boundary circumstances are elucidated mathematically. The physical pertinent parameters as shown in graphs and the friction factor, Nusselt number and Salts 1 and 2 Sherwood numbers are shown in surface plots. We observed that the momentum slip parameter decelerates the skin friction coefficient in the presence of a magnetic field and enhances in the absence of the magnetic field parameter. The thermal slip parameter enhances the Nusselt number in both the presence and absence of magnetic field parameter. Finally, the thermal and concentration buoyancy ratio parameters are shown to upsurge

the friction factor, Nusselt and Salts 1 and 2 Sherwood numbers in both cases of $M = 0$ and $M = 1$.

Keywords: thermal slip; momentum slip; Lie group transformations; triple diffusive convection; buoyancy forces; magnetohydrodynamic.
Mathematics Subject Classification: 76–10, 76R10

Nomenclature

u and v	Fluid velocities corresponding in x and y-directions
a	The rate of stretching sheet
L	The momentum slip parameter
V	The thermal slip factor
ψ	Stream function
$r_1, r_2, r_3, r_4, r_5, r_6$	Any constant real arbitrary parameter
η	Similarity variable
$f', \theta, \phi_1, \phi_2$	Dependent variables
α_1	Momentum slip parameter
α_2	Thermal slip parameter
τ_w	Shear stress
q_w	Heat flux
h_{1m} and h_{2m}	Mass flux
Le_1 and Le_2	Lewis numbers
ϕ_1	Salt 1 concentration
ϕ_2	Salt 2 concentration
Λ_1	Thermal buoyancy ratio parameter
Λ_2	Solutal buoyancy ratio parameter
M	Magnetic field parameter
T	Temperature of the fluid
C	Concentration of the fluid
β_T	Thermal buoyancy
β_{C_1}	Solutal 1 buoyancy
β_{C_2}	Solutal 2 buoyancy
$C_{1\infty}$ and $C_{2\infty}$	Solutal 1and 2 at ambient flow
ν	Kinematic viscosity of the fluid
Pr	Prandtl number
θ	Temperature
g	Gravity
ε	Small parameter
$\lambda > 0$	Buoyancy assisting flow
$\lambda < 0$	Buoyancy opposing flow

C_f	Local friction factor
Nu_x	Local Nusselt number
Sh_x^1 and Sh_x^2	Local Sherwood numbers
C_{1w} and C_{2w}	Concentrations 1 and 2 at the wall
Re_x	Reynolds number
α	Thermal diffusivity
D_{s_1} and D_{s_2}	Mass 1 and 2 diffusivities

1. Introduction

Lie group transformation or scaling group transformation has elements which are arbitrary close to the identity transformation, which means that the identity transformation is a transformation that changes nothing at all. When two mechanisms contributing to the density diffuse at different rates, convective waves can arise in a steadily stratified liquid. Sophus Lie's [1] was developed a differential invariant similarity for the Lie-group. His work was almost forgotten because of the growth of group theory and differential geometry to study differential equations [2]. Using Jeffrey and cross fluid models Bhatti et al. [3] and Sumer et al. [4] analysed importance of momentum with Lie group transformation. Numerical simulation of a thermally enhanced electro-magnetohydrodynamic (EMHD) flow of a heterogeneous micropolar mixture comprising (60%)-ethylene glycol, (40%) water, and copper oxide nanomaterials was studied by Shah et al. [5] and MHD heat transfer in thermal slip using semi-infinite domain and Carreau fluid has been discussed by Rehman et al. [6]. In recent year, so many researchers made their studies on Lie group transformation [7–9]. A two-component modeling for non-Newtonian nanofluid slips flow and heat transfer over sheet discussed by Rana et al. [10]. They observed that the heat transfer is decreases with increase in Brownian motion and thermophoresis parameters. Amanulla et al. [11] studied the numerical analysis of magnetohydrodynamic Williamson nanofluid over an isothermal sphere in the presence of momentum and thermal slip effects. Zhang et al. [12] proposed a new multi-view clustering model called Consensus Multi-view Clustering (CMC) model, and it is based on non-negative matrix factorization for predicting the multiple stages of Arithmetic design progression. The proposed CMC model performs multi-view learning to fully capture data features with limited medical images, analyzes similarity relations between different entities, addresses the shortcoming of multi-view fusion that requires manual setting parameters, and further acquires a consensus representation containing shared features and complementary knowledge of multiple view data. Later, Batool et al. [13] performed a numerical analysis of heat and mass transfer in micropolar nanofluids flow through a lid-driven cavity by using the finite volume method. They found that a high vortex viscosity parameter produces a weak concentration field and has significant behaviour when the Reynolds number is significant. Maneengam et al. [14] analyzed the entropy generation in a two-dimensional Lid-Driven porous container in the presence of obstacles of different shapes and under the influences of buoyancy and Lorentz forces. They concluded that the triangular shape of the baffle is the best in terms of thermal activity and also they observed that increasing the number of lower-wall waves reduces thermal activity. Bhutta et al. [15] experimentally investigated the development of novel hybrid two-dimensional and three-dimensional graphene oxide diamond microcomposite polyimide films to ameliorate electrical and thermal conduction. They found that the hybrid fillers with high

thermal and low electrical conductivities were responsible for synergistic improvements in the experimental results.Rasool et al. [16] performed a numerical investigation of electromagnetohydrodynamic nanofluid flows over a convectively heated Riga pattern positioned horizontally in a Darcy-Forchheimer porous medium. They observed that Darcy-Forchheimer's and Lorentz's forces strengthen the resulting frictional factor at the Riga surface. Rasool et al. [17] reported on the Darcy-Forchheimer flow of water conveying multi-walled carbon nanoparticles through a vertical Cleveland z-staggered cavity subject to entropy generation. They found that the velocity of incompressible Darcy-Forchheimer flow at the middle vertical Cleveland Z-staggered cavity declines with a higher Reynolds number.

The phenomena of heat and mass transport associated with entropy production describe the triple diffusion process, which can be found in metallurgy, oceanography, and geophysics. When more than one salt is used in a combined heat and mass transfer, the salts interact and cause coupling effects. In recent years tremendous research activity has been dedicated to developing various fluid models by using the triple diffusive effect: for examples with numerous geometries and multiple body forces, the reader is referred to Arif et al. [18], Patil et al. [19], Nawaz et al. [20] and Manjappa et al. [21]. Such techniques used to investigate momentum, thermal and various effects have been discussed by Patil et al. [22]; also the roughness of a surface with the nanofluid is studied by Patil et al. [23].

The numerical studies incorporated for thermal and momentum slips by Xiong et al. [24] and Beg et al. [25]. Su et al. [26] investigated that increasing flow and convective heat transmission were explored numerically inside circular and parallel-plates micro channels. The slip flow of conductive viscoelastic flow past a permeable radiated shrinking or stretching surface with mass transpiration has been illustrated by Sneha et al. [27]. The significance of nanoparticle shape and thermo-hydrodynamic slip constraints on MHD alumina-water nanoliquid flows over a rotating heated disk has been discussed by Sabu et al. [28]. Numerous researchers Koriko et al. [29], Eleni Seid et al. [30], Turkyilmazoglu [31], Felipe et al. [32], Majeed et al. [33] and Zeeshan et al. [34] are carried out for different fluid model with various surfaces to analyse the influence of momentum and thermal slips.

No research work has been done using Lie group transformation analysis to analyze the significance of triple diffusive convective flow by considering thermal and momentum slips, as per the authors' knowledge of the literature in most practical uses; however, the components of mass and heat are inextricably linked. The heat and mass diffusion components, on the other hand, are invariably coupled in most real-world applications. Triple diffusion of a fluid has practical applications in many bioengineering and medical sciences. For instance, aqueous suspensions of DNA contain more than two independently diffusing constituents with dissimilar diffusivities and medical drug manufacturing methods etc. However, triple diffusion in the presence of an applied magnetic field has significant applications in metallurgy, solar physics, geophysics, cosmic fluid dynamics, polymer industry, in the motion of the earth's core. This fact prompts us to investigate the combined impact of mass diffusion heat on magnetohydrodynamic free-convective flow in the boundary layer. As far as we can tell, the findings of this work appear to be perfectly consistent with previous research and, due to their simplicity, easily transferable to relevant applications.

2. Mathematical model and formulation

We perform the analysis of the steady triple diffusive hydromagnetic flow of heat and mass

transmission of a viscous, electrically conducting fluid. The flow is supposed to be in the *x*-direction and *y*-axis perpendicular to it. A uniform magnetic field of strength *B* is offered perpendicular to the flow direction. It is also considered that all fluid possessions are fixed excluding the impact of the density deviation with temperature and concentration. The surface is retained at a fixed temperature T_w, which is greater than the constant.

For this study, we have considered a triple diffusive free convective MHD incompressible flow with momentum and thermal slip conditions for a fluid model with the help of Lie group transformation analysis. Also, suppose that the flow generation is estimated for a linear widening surface. Additionally, the flow is restricted to the region $y > 0$ and equivalent with the plane $y = 0$.

Under the pre-defined assumptions mentioned above, the governing system of continuity, energy, momentum and concentration are expressed as follows:

$$\frac{\partial \bar{u}}{\partial \bar{x}} + \frac{\partial \bar{v}}{\partial \bar{y}} = 0\,, \tag{1}$$

$$\bar{u}\frac{\partial \bar{u}}{\partial \bar{x}} + \bar{v}\frac{\partial \bar{u}}{\partial \bar{y}} = \nu\frac{\partial^2 \bar{u}}{\partial \bar{y}^2} + \left[g\beta_T\left(T - T_\infty\right) + g\beta_{C_1}\left(C - C_{1\infty}\right) + g\beta_{C_2}\left(C - C_{2\infty}\right) - \frac{\sigma B^2}{\rho}\bar{u} \right], \tag{2}$$

$$\bar{u}\frac{\partial \bar{T}}{\partial \bar{x}} + \bar{v}\frac{\partial \bar{T}}{\partial \bar{y}} = \alpha\frac{\partial^2 \bar{T}}{\partial \bar{y}^2}\,, \tag{3}$$

$$\bar{u}\frac{\partial C_1}{\partial \bar{x}} + \bar{v}\frac{\partial C_1}{\partial \bar{y}} = D_{S_1}\frac{\partial^2 C_1}{\partial \bar{y}^2}\,, \tag{4}$$

$$\bar{u}\frac{\partial C_2}{\partial \bar{x}} + \bar{v}\frac{\partial C_2}{\partial \bar{y}} = D_{S_1}\frac{\partial^2 C_2}{\partial \bar{y}^2}\,, \tag{5}$$

Given the following boundary conditions:

$$\begin{aligned} &\bar{u} = a\bar{x} + L\frac{\partial u}{\partial y}, \bar{v} = 0, T = T_w + D_1\frac{\partial T}{\partial y}, C_1 = C_{1w}, C_2 = C_{2w} \text{ at } \eta = 0 \\ &\bar{u} \to u_\infty, T \to T_\infty, C_1 \to C_{1\infty}, C_2 \to C_{2\infty} \text{ as } \eta \to \infty \end{aligned}\,, \tag{6}$$

Now, we need to transform the above Eqs (1) to (6) into non-dimensional form. To perform this, the following similarity dimensionless transformations are considered.

$$\begin{aligned} &u = \frac{\bar{u}}{\sqrt{a\nu}}, v = \frac{\bar{v}}{\sqrt{a\nu}}, x = \frac{\bar{x}}{\sqrt{\nu/a}}, y = \frac{\bar{y}}{\sqrt{\nu/a}} \\ &\theta = \frac{T - T_\infty}{T_w - T_\infty}, \phi_1 = \frac{C_1 - C_{1\infty}}{C_{1w} - C_{1\infty}}, \phi_2 = \frac{C_2 - C_{2\infty}}{C_{2w} - C_{2\infty}} \end{aligned}\,, \tag{7}$$

We substitute the above non-dimensional quantities of (7) in Eqs (1) to (5) along with the boundary conditions of Eq (6) and then complete the simplification results by using the following

non-dimensional differential equations :

$$\frac{\partial u}{\partial x}+\frac{\partial v}{\partial y}=0\,, \tag{8}$$

$$u\frac{\partial u}{\partial x}+v\frac{\partial u}{\partial y}=\frac{\partial^2 u}{\partial y^2}-\frac{\sigma B^2}{\rho a}u+\lambda\theta+\Lambda_1\phi_1+\Lambda_2\phi_2\,, \tag{9}$$

$$u\frac{\partial \phi_1}{\partial x}+v\frac{\partial \phi_1}{\partial y}=\frac{D_{S_1}}{\nu}\frac{\partial^2 \phi_1}{\partial y^2}\,, \tag{10}$$

$$u\frac{\partial \phi_1}{\partial x}+v\frac{\partial \phi_1}{\partial y}=\frac{D_{S_1}}{\nu}\frac{\partial^2 \phi_1}{\partial y^2}\,, \tag{11}$$

$$u\frac{\partial \phi_2}{\partial x}+v\frac{\partial \phi_2}{\partial y}=\frac{D_{S_2}}{\nu}\frac{\partial^2 \phi_2}{\partial y^2}\,, \tag{12}$$

with the following boundary conditions :

$$\begin{aligned} &u=x+L\sqrt{\frac{a}{\nu}}\frac{\partial u}{\partial y}, v=0, \theta=1+D_1\sqrt{\frac{a}{\nu}}\frac{\partial \theta}{\partial y}, \phi_1=1, \phi_2=1 \text{at}\ \eta=0\\ &u\to 0, \theta\to 0, \phi_1\to 0, \phi_2\to 0 \text{ as } \eta\to\infty \end{aligned}\,, \tag{13}$$

where $\lambda=\frac{g\beta_T\Delta T}{a\sqrt{a\nu}}, \Lambda_1=\frac{g\beta_{C_1}\Delta C_1}{a\sqrt{a\nu}}, \Lambda_1=\frac{g\beta_{C_2}\Delta C_2}{a\sqrt{a\nu}}$.

3. Scaling transformations

First, the stream function ψ is taken as mentioned below before applying scaling transformations.

$$u=\frac{\partial \psi}{\partial y} \text{and} \, u=-\frac{\partial \psi}{\partial x} \tag{14}$$

We introduce the stream functions (14) to (8)–(12) together with the boundary conditions of (13). Obviously, Eq (8) is satisfied by them. And the remaining equations will be converted in terms of the stream function ψ as below period:

$$\frac{\partial \psi}{\partial x}\frac{\partial^2 \psi}{\partial x\partial y}-\frac{\partial \psi}{\partial x}\frac{\partial^2 \psi}{\partial y^2}=\frac{\partial^3 \psi}{\partial y^3}-\frac{\sigma B^2}{\rho a}\frac{\partial \psi}{\partial y}-\lambda\theta+\Lambda_1\phi_1+\Lambda_2\phi_2\,, \tag{15}$$

$$\frac{\partial \psi}{\partial y}\frac{\partial \theta}{\partial x}-\frac{\partial \psi}{\partial x}\frac{\partial \psi}{\partial y}=\frac{\alpha}{\nu}\frac{\partial^2 \theta}{\partial y^2}\,, \tag{16}$$

$$\frac{\partial \psi}{\partial y}\frac{\partial \phi_1}{\partial x}-\frac{\partial \psi}{\partial x}\frac{\partial \phi_1}{\partial y}=\frac{D_{S_1}}{\nu}\frac{\partial^2 \phi_1}{\partial y^2}, \tag{17}$$

$$\frac{\partial \psi}{\partial y}\frac{\partial \phi_2}{\partial x}-\frac{\partial \psi}{\partial x}\frac{\partial \phi_2}{\partial y}=\frac{D_{S_2}}{\nu}\frac{\partial^2 \phi_2}{\partial y^2}, \tag{18}$$

with the following boundary conditions:

$$\begin{aligned}&\frac{\partial \psi}{\partial y}=x+L\sqrt{\frac{a}{\nu}}\frac{\partial^2 \psi}{\partial y^2},\frac{\partial \psi}{\partial x}=0,\theta=1+D_1\sqrt{\frac{a}{\nu}\frac{\partial \theta}{\partial y}},\phi_1=1,\phi_2=1\text{at}\,\eta=0\\&\frac{\partial \psi}{\partial y}\to 0,\theta\to 0,\phi_1\to 0,\phi_2\to 0\text{as}\;\eta\to\infty\end{aligned}, \tag{19}$$

$$\text{Also, } e^{\varepsilon(r_2-r_3)}\frac{\partial \psi^*}{\partial y^*}=1, e^{\varepsilon(r_1-r_3)}=0, e^{\varepsilon r_4}\theta^*=0 \tag{20}$$

Consider ε as a small parameter of the scaling transformation. Then, the transformation F (a specified set of Lie group analysis) is taken as mentioned below period:

$$\begin{aligned}&F: x^*=xe^{\varepsilon r_1}, y^*=ye^{\varepsilon r_2}, \psi^*=\psi e^{\varepsilon r_3}\\&\theta^*=\theta e^{\varepsilon r_4}, \phi_1^*=\phi_1 e^{\varepsilon r_5}, \phi_2{}^*=\phi_2 e^{\varepsilon r_6}\end{aligned}, \tag{21}$$

Where, r_1, r_2, r_3, r_4, r_5 and r_6 are any real arbitrary constant parameters The point conversion defined through (21) transmuted the co-ordinates $\left(x, y, \psi, \phi_1, \phi_2\right)$ into $\left(x^*, y^*, \psi^*, \phi_1^*, \phi_2^*\right)$. With the help of Lie group analysis mentioned through (15), Eqs (15)–(18) are transformed as

$$e^{\varepsilon(r_1+r_2-r_3-r_5)}\left[\frac{\partial \psi^*}{\partial y^*}\frac{\partial^2 \psi^*}{\partial x^*\partial y^*}-\frac{\partial \psi^*}{\partial x^*}\frac{\partial^2 \psi^*}{\partial y^{*2}}\right]=e^{\varepsilon(3r_2-r_3)}\frac{\partial^3 \psi^*}{\partial y^{*3}}-e^{\varepsilon(r_2-r_3)}\frac{\sigma B^2}{\rho a}\frac{\partial \psi^*}{\partial y^*}-\lambda e^{\varepsilon r_4}\theta \tag{22}$$

$$e^{\varepsilon(r_1+r_2-r_3-r_5)}\left[\frac{\partial \psi^*}{\partial y^*}\frac{\partial^2 \theta^*}{\partial x^*\partial y^*}-\frac{\partial \psi^*}{\partial x^*}\frac{\partial \theta^*}{\partial y^*}\right]=\frac{a}{\nu}e^{\varepsilon(2r_2-r_4)}\frac{\partial^2 \theta^*}{\partial y^{*2}} \tag{23}$$

$$e^{\varepsilon(r_1+r_2-r_3-r_5)}\left[\frac{\partial \psi^*}{\partial y^*}\frac{\partial \phi_1^*}{\partial x^*}-\frac{\partial \psi^*}{\partial x^*}\frac{\partial \phi_1^*}{\partial y^*}\right]=\frac{D_{S_1}}{\nu}e^{\varepsilon(2r_2-r_5)}\frac{\partial^2 \phi_1^*}{\partial y^{*2}} \tag{24}$$

$$e^{\varepsilon(r_1+r_2-r_3-r_6)}\left[\frac{\partial \psi^*}{\partial y^*}\frac{\partial \phi_2{}^*}{\partial x^*}-\frac{\partial \psi^*}{\partial x^*}\frac{\partial \phi_2{}^*}{\partial y^*}\right]=\frac{D_{S_2}}{\nu}e^{\varepsilon(2r_2-r_6)}\frac{\partial^2 \phi_2{}^*}{\partial y^{*2}}. \tag{25}$$

If the exponent of the above converted equations fulfills the below linear equations, then the set of Eqs (22)–(25) will remain invariant under the folowing transformation

$$r_1 = 2r_2 - 2r_3 = 3r_2 - r_3 = r_2 - r_3 = r_4 = r_5 = r_6, \tag{26}$$

$$r_1 + r_2 - r_3 - r_4 = 2r_2 - r_4, \tag{27}$$

$$r_1 + r_2 - r_3 - r_5 = 2r_2 - r_5, \tag{28}$$

$$r_1 + r_2 - r_3 - r_6 = 2r_2 - r_6 \tag{29}$$

By solving the above linear equations (26)–(29) simultaneously, we find

$$r_1 = r_1, r_2 = 0, r_3 = r_1, r_4 = 0, r_5 = 0, r_6 = 0. \tag{30}$$

Replacing the above values of (30) into the scaling transformations given in (21), we get

$$F : x^* = xe^{\varepsilon r_1}, y^* = y, \psi^* = \psi e^{\varepsilon r_1}, \theta^* = \theta, \phi_1^* = \phi_1, \phi_2^* = \phi_2. \tag{31}$$

The Taylor series expansions are

$$x^* - x = x\varepsilon r_1, y^* - y = 0, \psi^* = \psi\varepsilon r, \theta^* - \theta = 0, \phi_1^* - \phi_1 = 0, \phi_2^* - \phi_2 = 0.$$

A simple algebraic expression for the above transformations given by (31) with the help of Taylor series expansion leads to a mono-parametric group of transformations in the form of the characteristic equation given below period

$$\frac{dx}{dr_1} = \frac{dy}{0} = \frac{d\psi}{\psi r_1} = \frac{d\theta}{0} = \frac{d\phi_1}{0} = \frac{d\phi_2}{0}. \tag{32}$$

From (32), we can easily obtain new similarity transformations as

$$y = \eta, \psi = xf(\eta), \theta = \theta(\eta), \phi_1 = \phi_1(\eta), \phi_2 = \phi_2(\eta), \tag{33}$$

where, η is the similarity variable and $f, \theta, \phi_1, \phi_2$ are the dependent variables. Now, we substitute the above quantities specified in (33) into PDEs (16) to (18) then, by applying the boundary conditions mentioned in (19), we attain the set of ordinary differential equations as

$$f''' + ff'' - f'^2 + \lambda\theta + \Lambda_1\phi_1 + \Lambda_2\phi_2 = 0, \tag{34}$$

$$\theta'' + \Pr\theta' = 0, \tag{35}$$

$$\phi_1'' + Le_1 f\phi_1' = 0, \tag{36}$$

$$\phi_2'' + Le_2 f \phi_2' = 0. \tag{37}$$

Together with the boundary situations;

$$\begin{aligned} &f = 0,\ f' = 1 + \alpha_1 f'', \theta = 1 + \alpha_2 \theta', \phi_1 = 1, \phi_2 = 1 \text{at} \ \eta = 0 \\ &f' \to 0, \theta \to 0, \phi_1 \to 0, \phi_2 \to 0 \ \text{as} \ \eta \to \infty \end{aligned} \tag{38}$$

Here, $\alpha_1 = L\sqrt{\frac{a}{\nu}}$ is the momentum slip parameter and $\alpha_2 = D_1\sqrt{\frac{a}{\nu}}$ is the thermal slip parameter. with the following predefined parameters:

$$M = \frac{\sigma B^2}{\rho a}, \lambda = \frac{g\beta_T \Delta T}{a\sqrt{a\nu}}, \Lambda_1 = \frac{g\beta_{C_1}\Delta C_1}{a\sqrt{a\nu}}, \Lambda_2 = \frac{g\beta_{C_2}\Delta C_2}{a\sqrt{a\nu}}, \Pr = \frac{\nu}{\alpha}, Le_1 = \frac{\nu}{D_{S_1}}, Le_2 = \frac{\nu}{D_{S_2}}.$$

The physical measures requiring engineering attention are the local friction factor; local Nusselt number and Sherwood number which are defined as follows:

$$C_f = \frac{\tau_w}{\rho(ax)^2}, Nu_x = \frac{xq_w}{k(T_w - T_\infty)}, Nu_x = \frac{xq_w}{k(T_w - T_\infty)}, Sh_x^{\ 1} = \frac{xh_m}{D_{sm}(C_{1w} - C_{1\infty})}, Sh_x^{\ 2} = \frac{xh_m}{D_{sm}(C_{2w} - C_{2\infty})},$$

where, τ_w, q_w, h_{1m} & h_{2m} symbolize the shear stress, heat and mass flux change, respectively:

$$\tau_w = -\mu\left(\frac{\partial u}{\partial y}\right), q_w = -k\left(\frac{\partial T}{\partial y}\right), h_{1m} = -D_{sm}\left(\frac{\partial C_1}{\partial y}\right), h_{2m} = -D_{sm}\left(\frac{\partial C_2}{\partial y}\right).$$

The dimensionless friction factor, Nusselt number and Sherwood number are defined as

$$C_f \ \mathrm{Re}_x^{\ 1/2} = f''(0), \frac{Nu_x}{\mathrm{Re}_x^{\ 1/2}} = -\theta'(0), \frac{Sh_{1x}}{\mathrm{Re}_x^{\ 1/2}} = -\phi_1'(0), \frac{Sh_{2x}}{\mathrm{Re}_x^{\ 1/2}} = -\phi_2'(0),$$

Where, $\mathrm{Re}_x = \sqrt{\frac{a}{\nu l}}x$.

4. Results and discussions

The collected results show the impact of non-dimensional regulating parameters such as $Le_1, Le_2, \Lambda_1, \Lambda_2, \alpha_1, \alpha_2$ on and $f'(\eta), \theta(\eta), \phi_1(\eta), \phi_2(\eta)$ (See Figures 1–16). In the simulations, the pertinent parameter values were $\Pr = 0.72, \lambda = -0.5, Le_1 = 1, Le_2 = 1, \Lambda_1 = 0.5, \Lambda_2 = 0.5, \alpha_1 = 0.2, \alpha_2 = 0.2$. These variables were kept constant throughout the inquiry, with the exception of the various values given in the associated figures. The results are compared with already divulged results and presents excellent correlation with the Ferdows et al. [35] results.

Table 1. Corroboration of $\theta'(0)$ for distinct values of Pr with $M = \lambda = Nc_1 = Nc_2 = Le_1 = Le_2 = 0$.

Pr	Ferdows et al. [35]	Present Results
1	0.9547	0.9546
2	1.4715	1.4711
3	1.8691	1.8672

The variation in salt 1 and 2 concentration distributions ϕ_1 and ϕ_2 as a result of varying the regular Lewis numbers Le_1 and Le_2 in the presence and absence of the magnetic field parameter are shown in Figures 1–4. It was designed to observe the impact of Lewis numbers on salt 1 and 2 concentrations. Decreases in the solutal concentration profiles ϕ_1 and ϕ_2 is occurred due to the Lewis number. Physical explanation of such decline in the variations of ϕ_1 and ϕ_2 can be justified on the fact that Le_1 and Le_2 capture the reverse relation with species diffusion, that is when Le_1 and Le_2 are maximum, species diffusion is lower, which leads to the decrement of the resulting solutal concentrations.

The thermal buoyancy ratio parameter Λ_1 reduces $f'(\eta), \theta(\eta), \phi_1(\eta), \phi_2(\eta)$ for both the presence and absence of a magnetic field. The concentration buoyancy ratio parameter Λ_2 enhances $\theta(\eta)$ in the presence of a magnetic field but slowly decelerates it in the absence of a magnetic field case (Figure 10). The effect of thermal the buoyancy ratio parameter Λ_1 is depicted in Figure 5. From this, we observed that with the increase of the velocity and temperature, Salt 1 and 2 concentration distributions decreased because molecular forces dominated the thermal buoyancy forces. Therefore, the velocity in the momentum boundary layer depreciates in the flow region when the buoyancy forces act in the opposite direction.

The momentum and concentration boundary layer thicknesses decreased the values of Λ_2 in both cases (see Figures 9, 11 and 12).

Figures 13–15 show the influence of the momentum slip parameter α_1 on the velocity, temperature and Salt 1 concentration distributions. It is clear that the velocity is a decreasing function of the slip parameter. Physically, when slip occurs, the fluid velocity near the surface is no longer equal to the surface velocity, that is, a velocity slip exists with such an increase in a slip velocity. Furthermore, increasing the value of slip will decrease the flow velocity because, under the slip condition, the pulling of the surface can be only partly transmitted to the fluid. The same phenomena can be observed in the temperature and Salt 1 concentration fields. Figure 16 demonstrates the effect of the thermal slip parameter α_2 on temperature. As the thermal slip parameter increases, less heat is transformed from the surface to the fluid and consequently the temperature decreases.

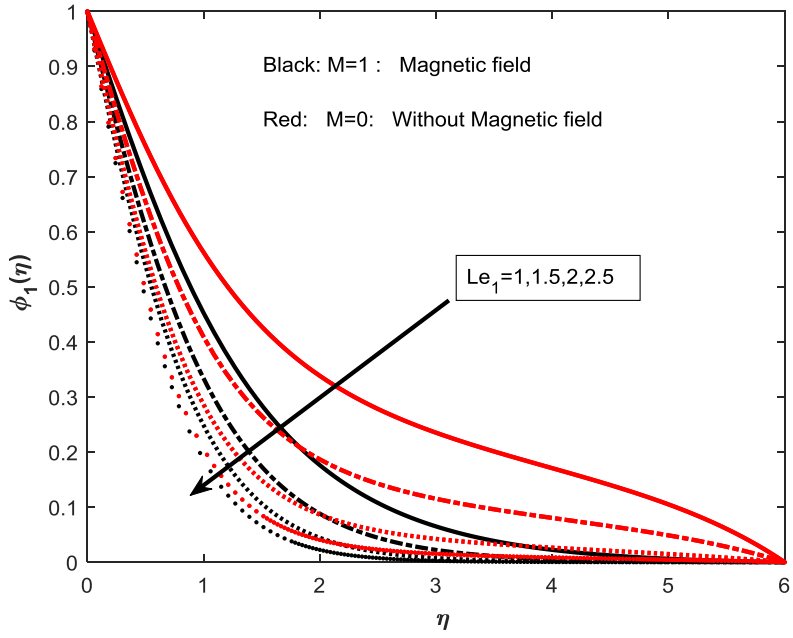

Figure 1. Salt 1 concentration on Le_1.

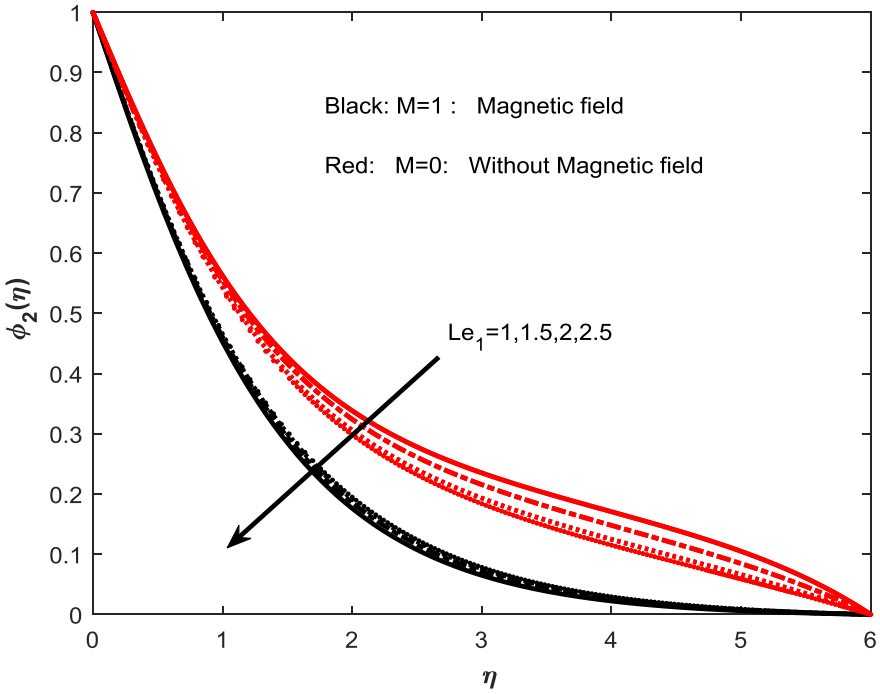

Figure 2. Salt 2 concentration on Le_1.

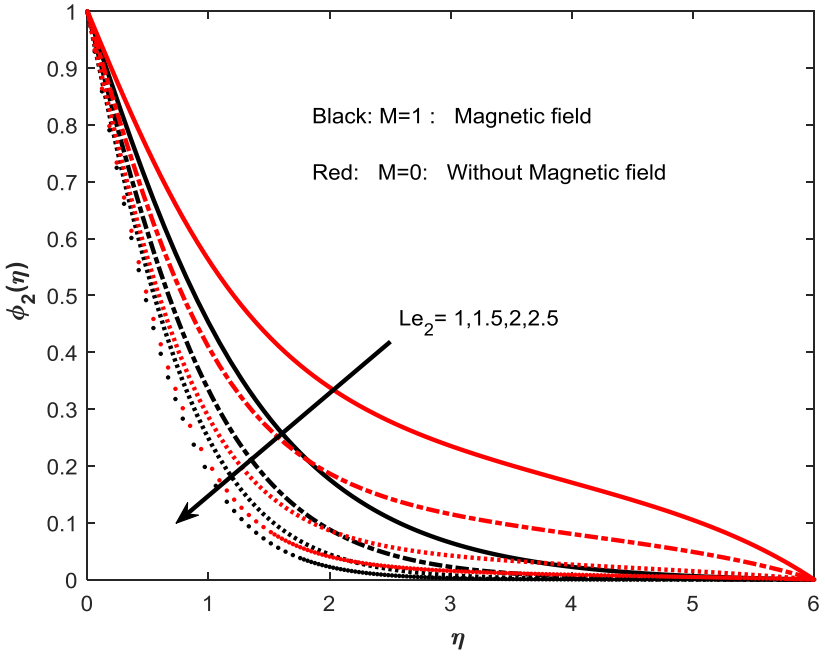

Figure 3. Salt 2 concentration on Le_2.

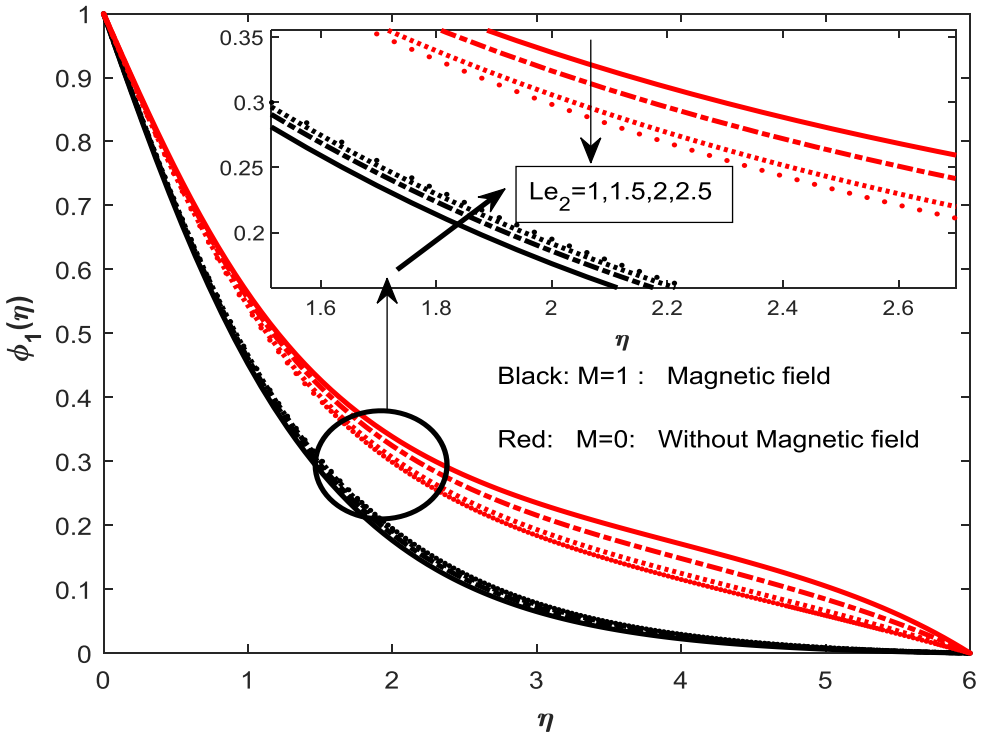

Figure 4. Salt 1 concentration on Le_2.

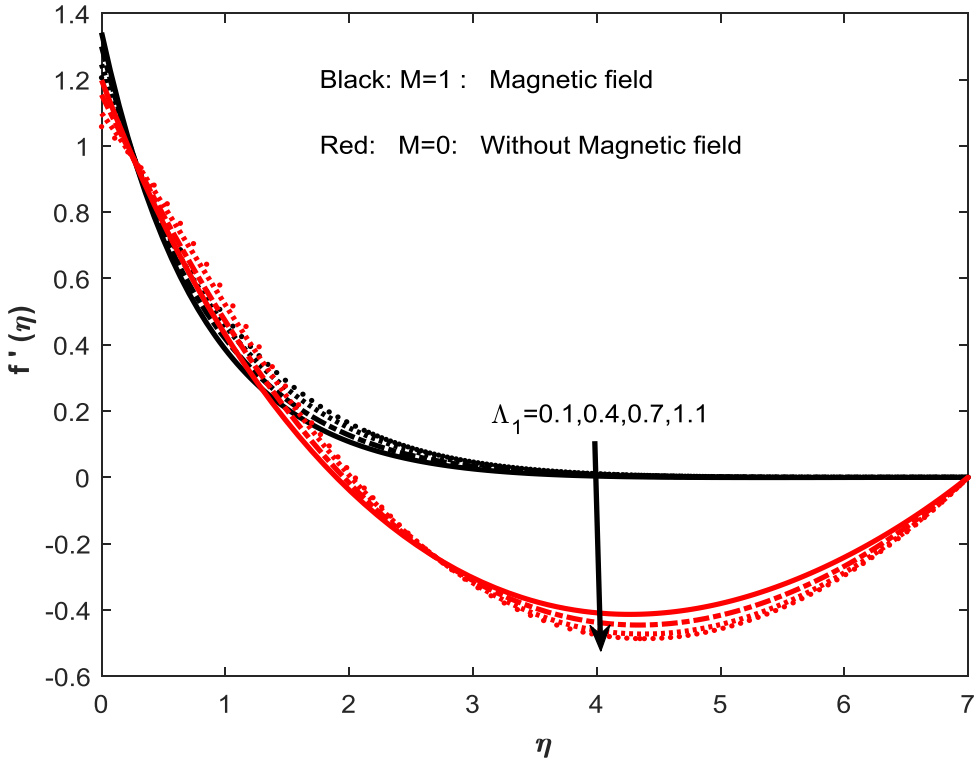

Figure 5. Velocity on Λ_1.

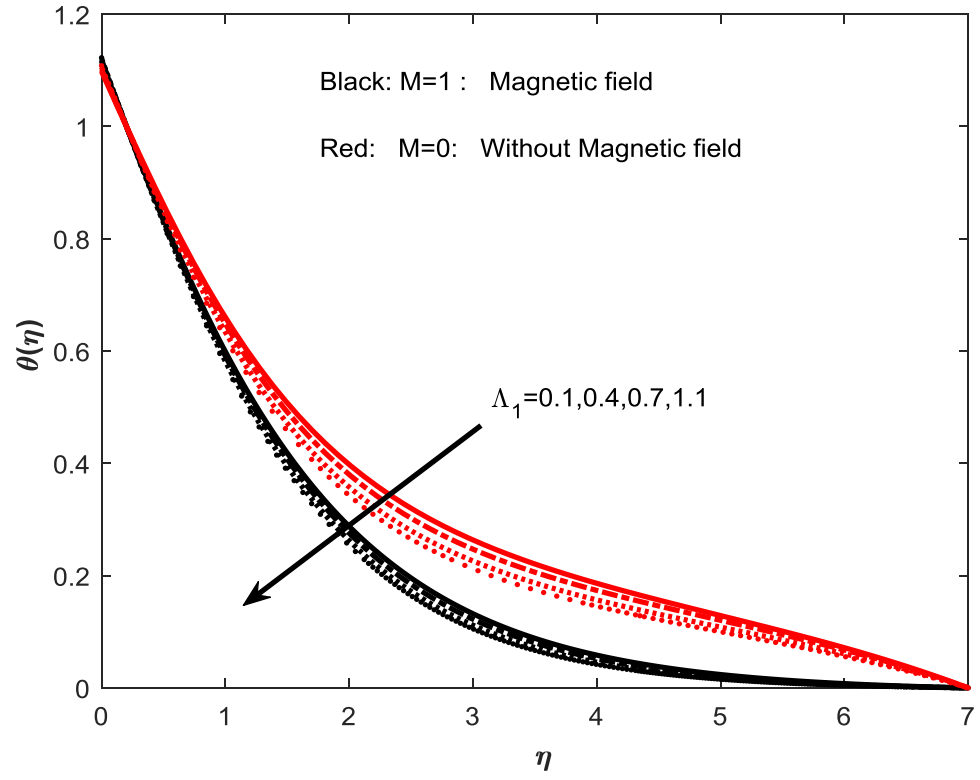

Figure 6. Temperature on Λ_1.

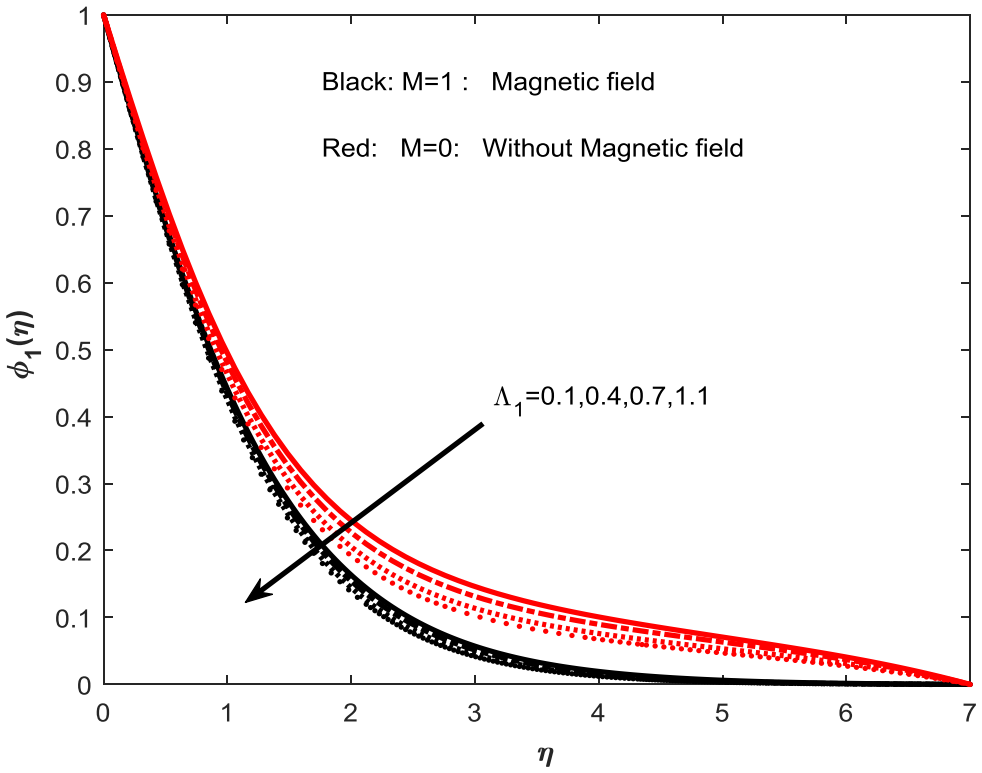

Figure 7. Salt 1 concentartion on Λ_1.

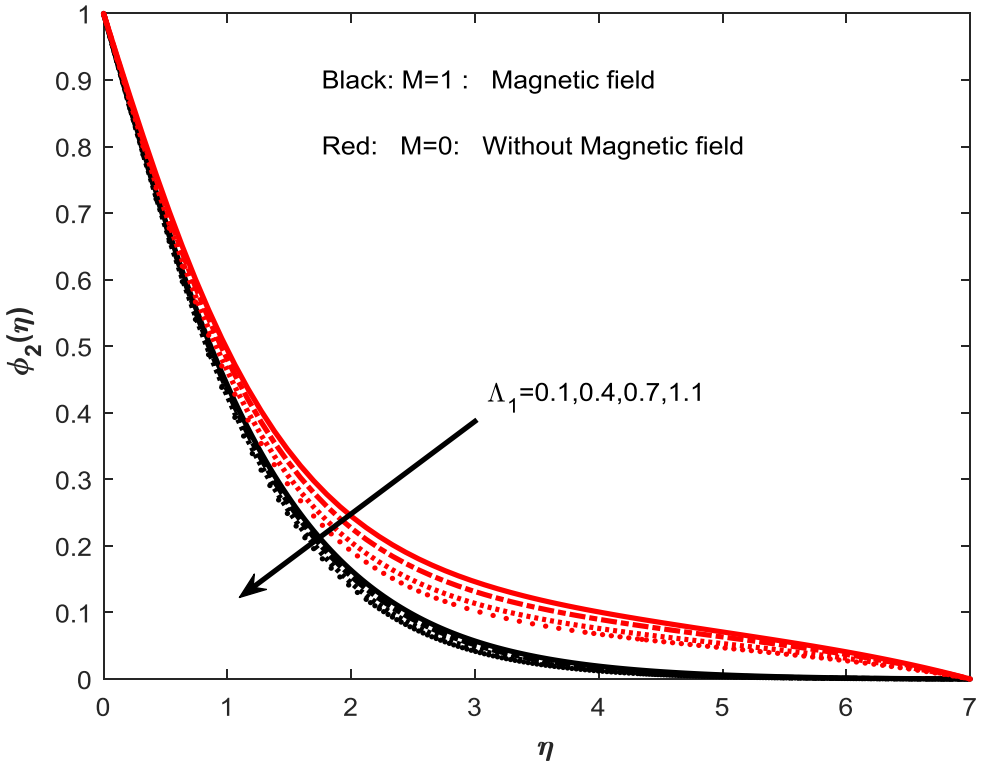

Figure 8. Salt 2 concentration on Λ_1.

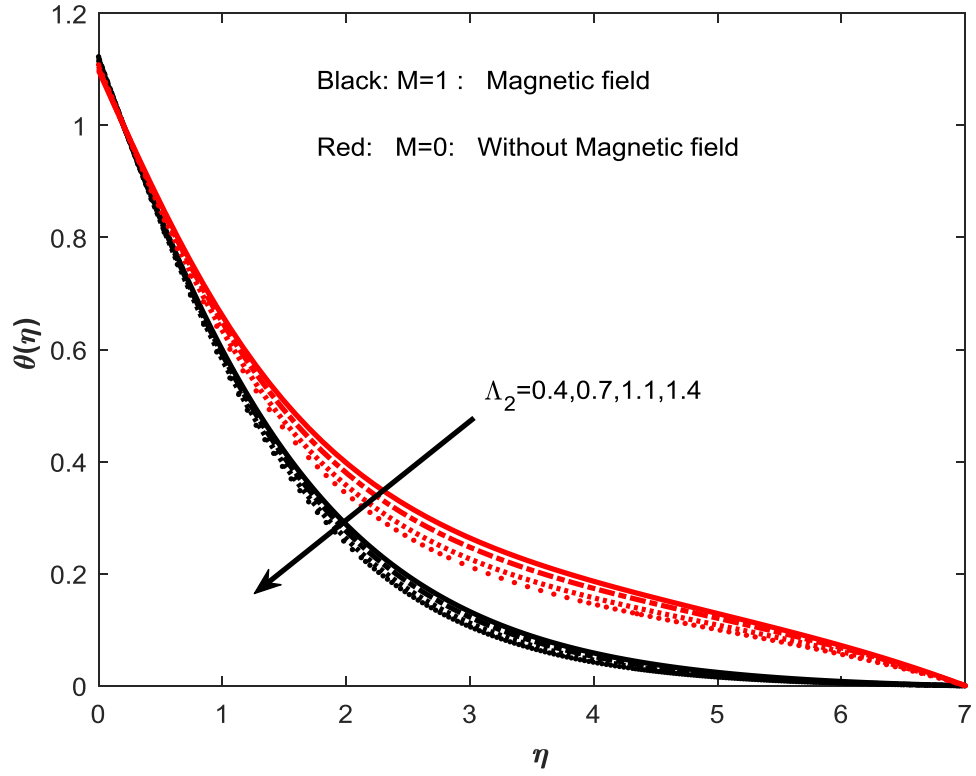

Figure 9. Temperature on Λ_2.

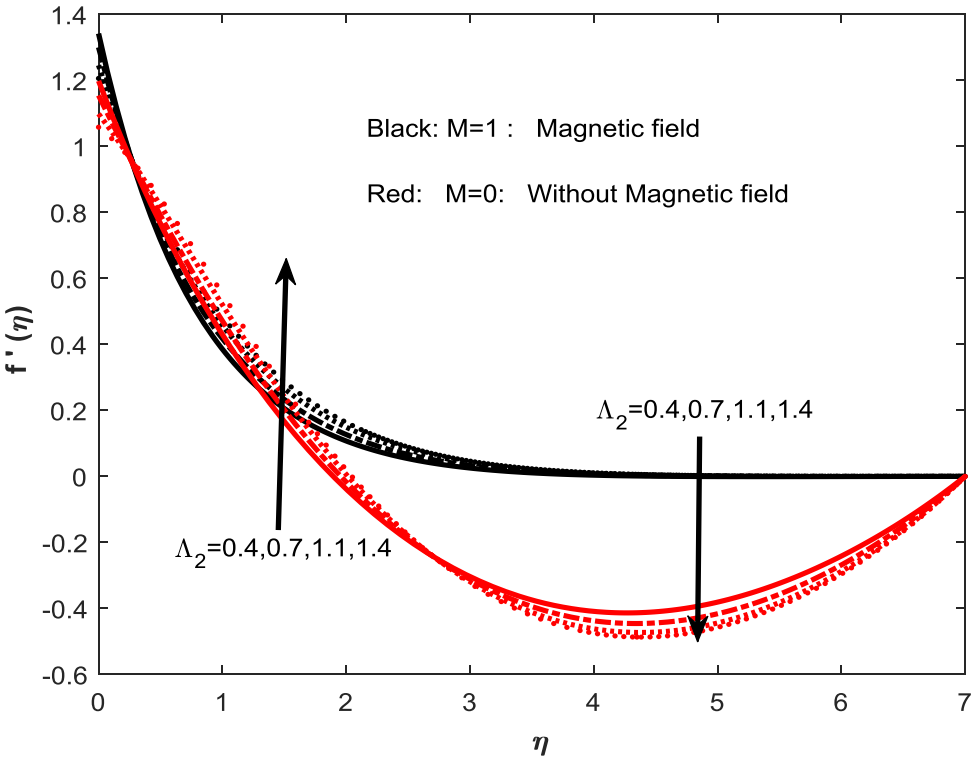

Figure 10. Velocity on Λ_2.

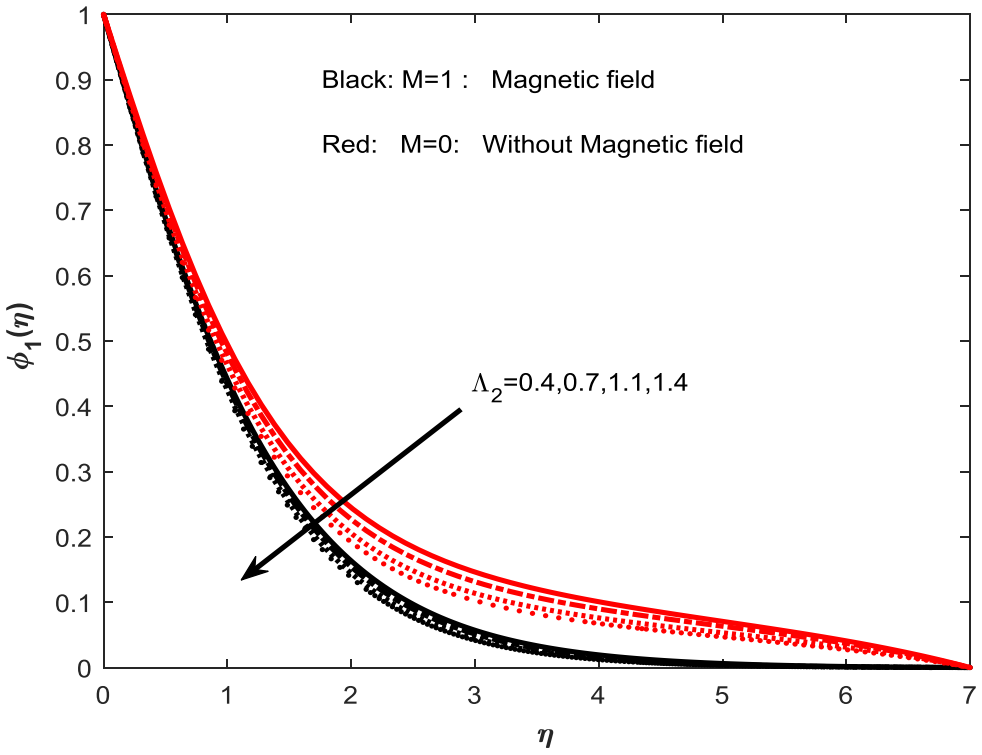

Figure 11. Salt 1 concentration on Λ_2.

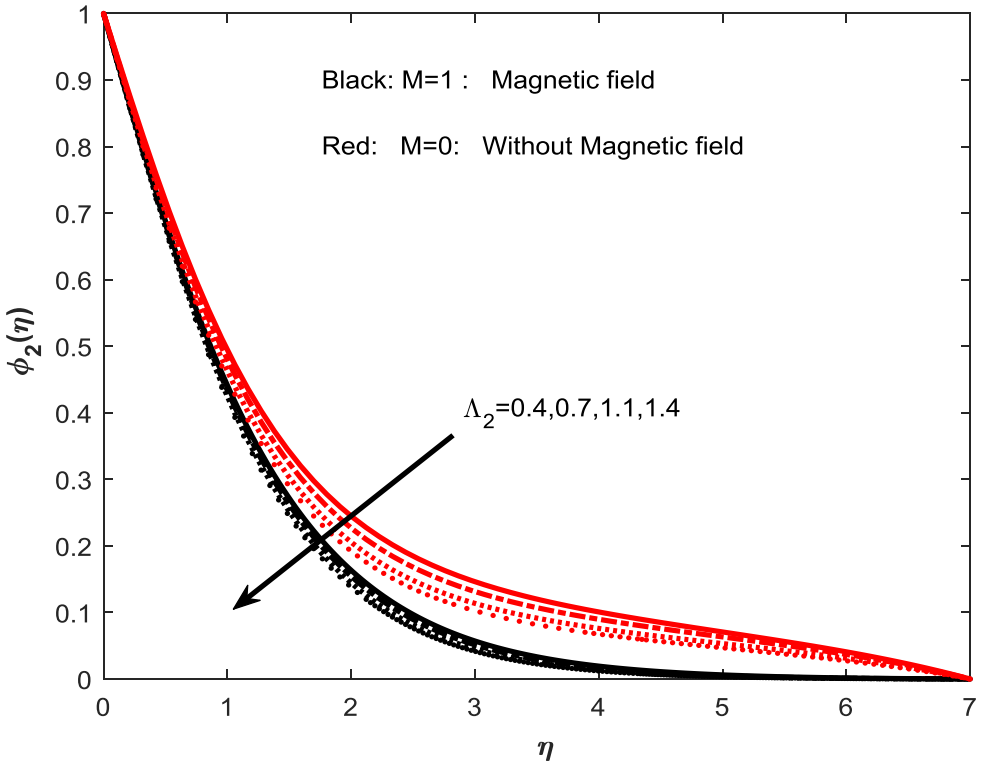

Figure 12. Salt 2 concentration on Λ_2.

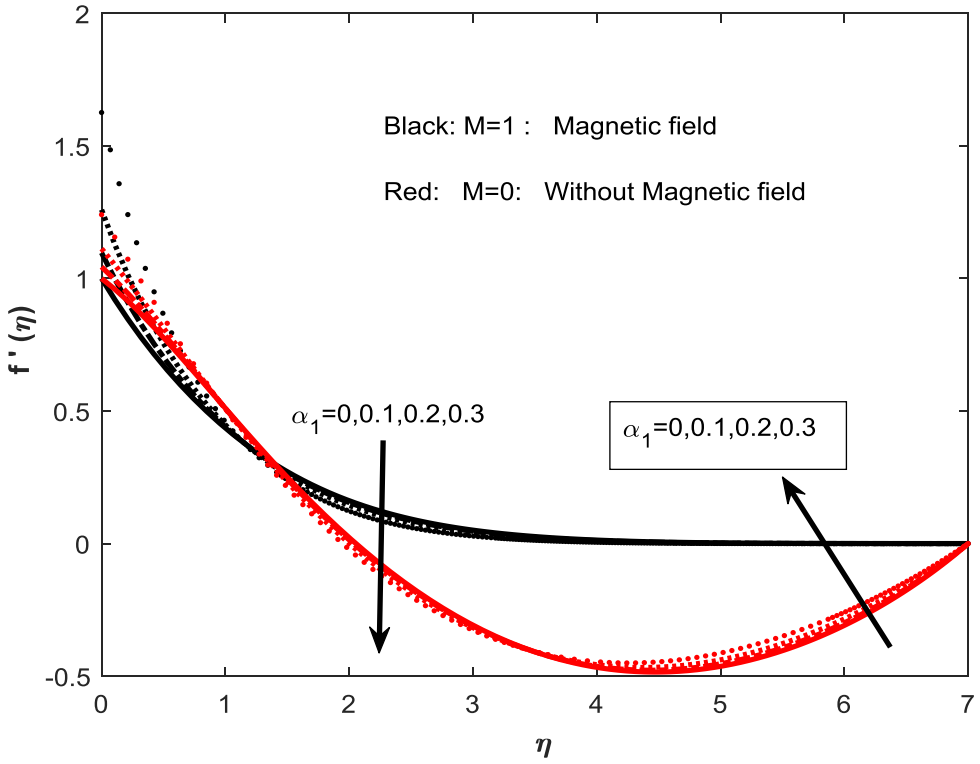

Figure 13. Velocity on α_1.

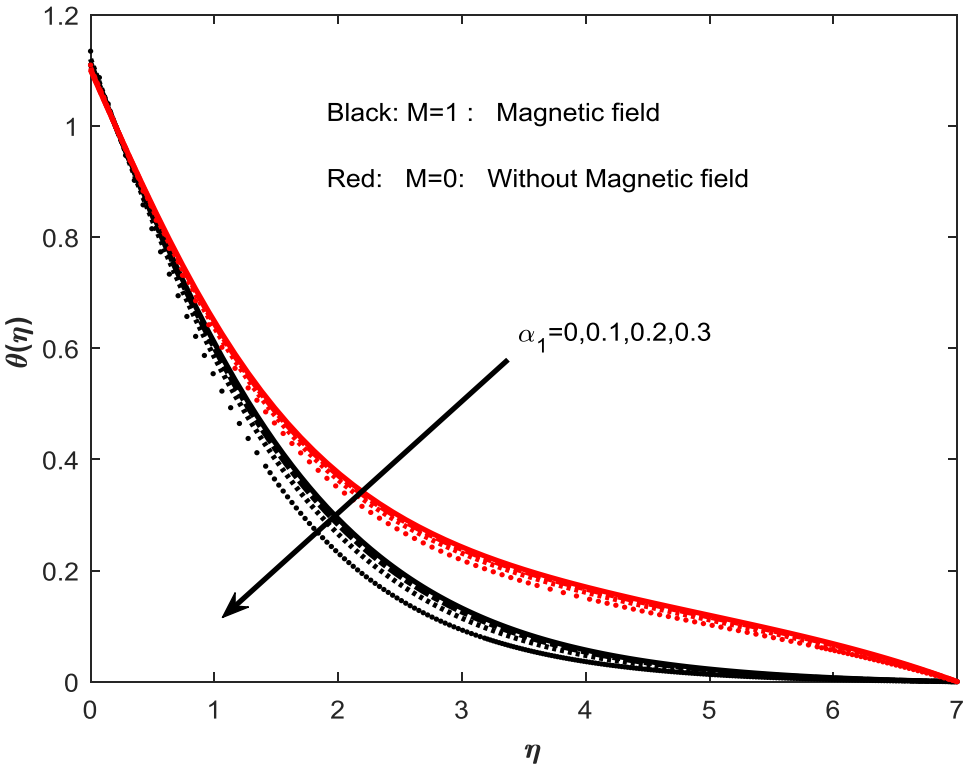

Figure 14. Temperature on α_1.

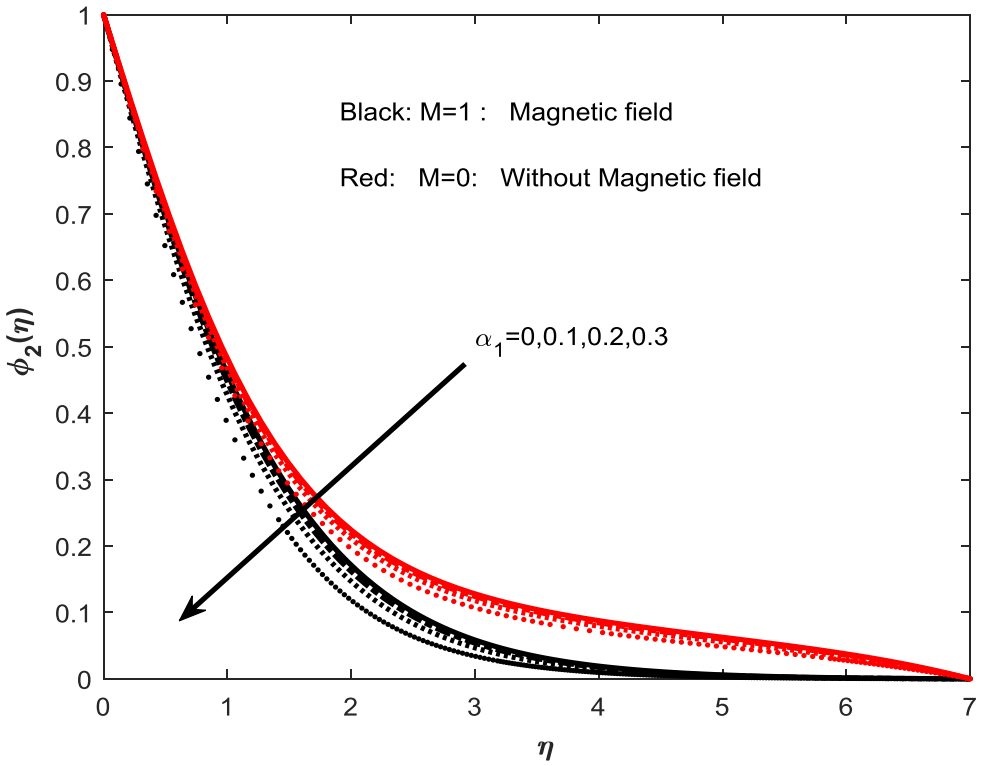

Figure 15. Salt 2 concentration on α_1.

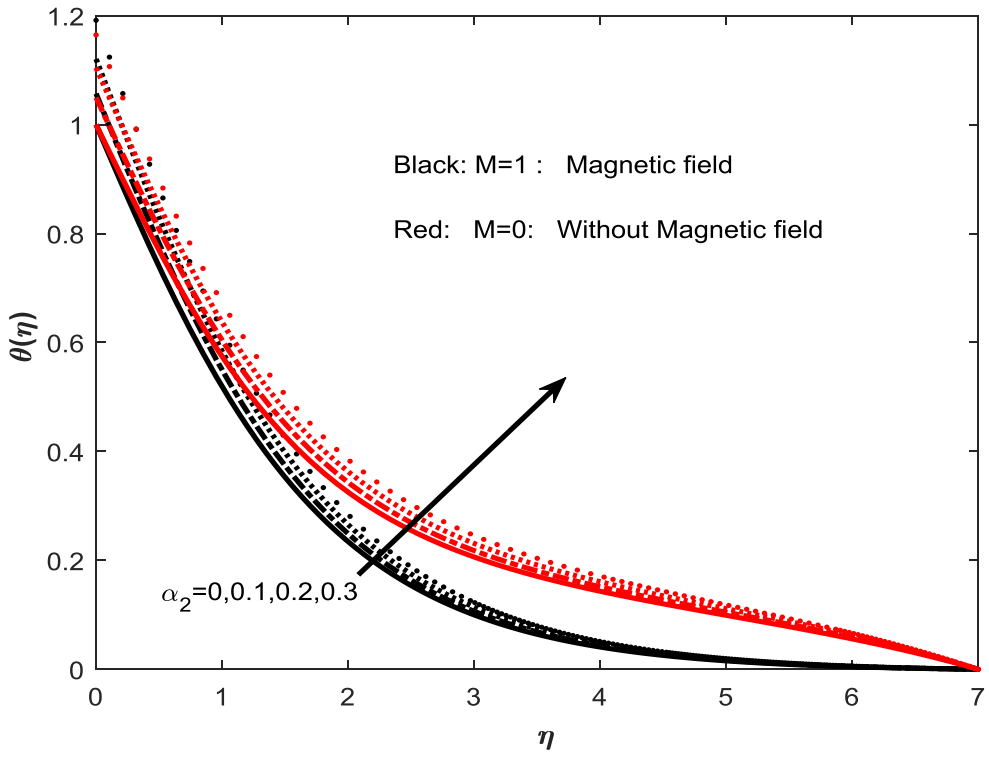

Figure 16. Temperature on α_2.

Figure 17 represents the surface plot of the momentum slip parameter α_1 given the skin friction coefficient $f''(0)$, Nusselt number $\theta'(0)$ and Sherwood number $\phi'(0)$ in the absence of the magnetic field parameter $M=0$ and presence of the magnetic field parameter $M=1$. Figure 17 shows that the rate of friction factor is −4.256939 in the absence of a magnetic field and −1.454855 in the presence a of magnetic field case. From this we observed that the friction factor coefficient continuously decreases. The opposite phenomena can be observed in the cases of the Nusselt and Sherwood numbers for both the $M=0$ and $M=1$ cases (Figures 18–20). Figure 21 represents the thermal slip parameter α_2 on $f''(0),\theta'(0),\phi'(0)$ for both absence and presence of magnetic field parameter cases. Figures 21 and 22 show that α_2 elevates the rate of heat transfer but decelerates the skin friction coefficient for both cases.

The concentration buoyancy ratio parameter Λ_2 escalates the Salt 1 Sherwood number (Figure 23) and thermal buoyancy ratio parameter Λ_1 also enhances the friction factor coefficient (Figure 24) for the $M=0$ and $M=1$ cases. Figure 25 shows that the Lewis number Le_1 reduces the Nusselt number in the $M=0$ case and increases the Nusselt number in the case of $M=1$ the same phenomena can be observed in Figure 27 Salt 2 Sherwood number. But the skin friction coefficient increases for both cases of magnetic field parameter settings, as shown in Figure 26. Finally, from Figures 28 and 31 we observed that Le_2 reduces the skin friction coefficient but upsurges the Salt 2 Sherwood number; meanwhile Le_2 in the absence of a magnetic field and increase in the presence of a magnetic field for the Nusselt number Salt 1 concentration, as shown in Figures 29 and 30.

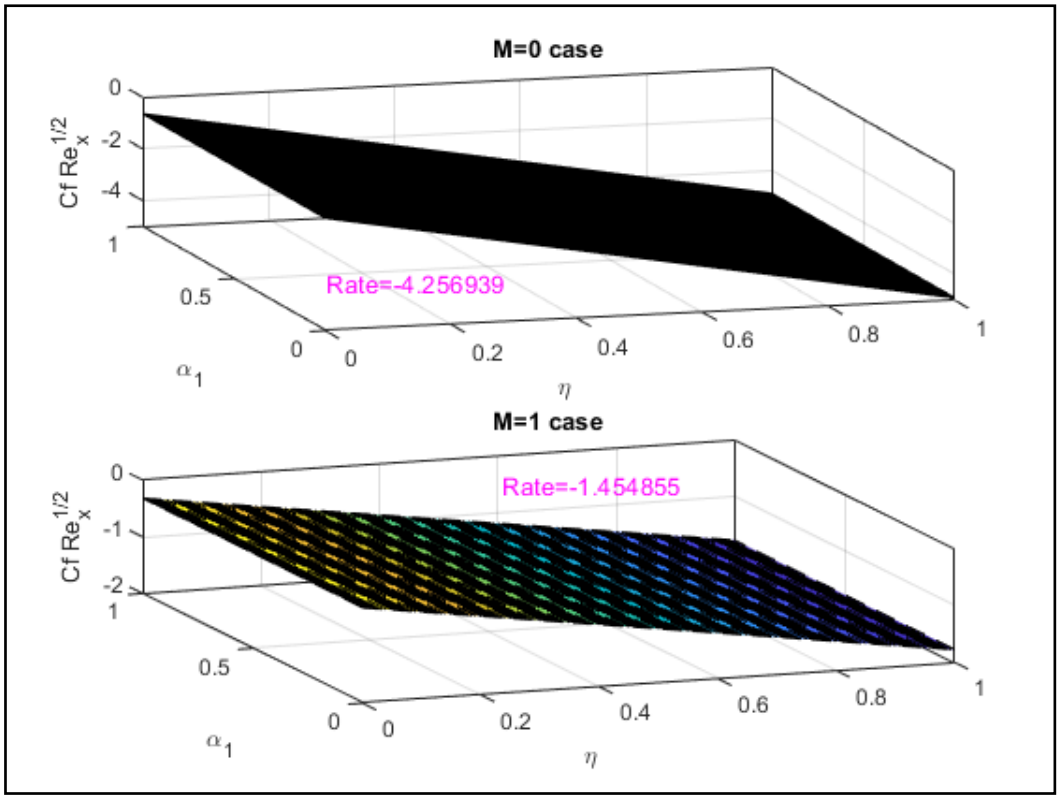

Figure 17. Surface plot of skin friction coefficient on α_1.

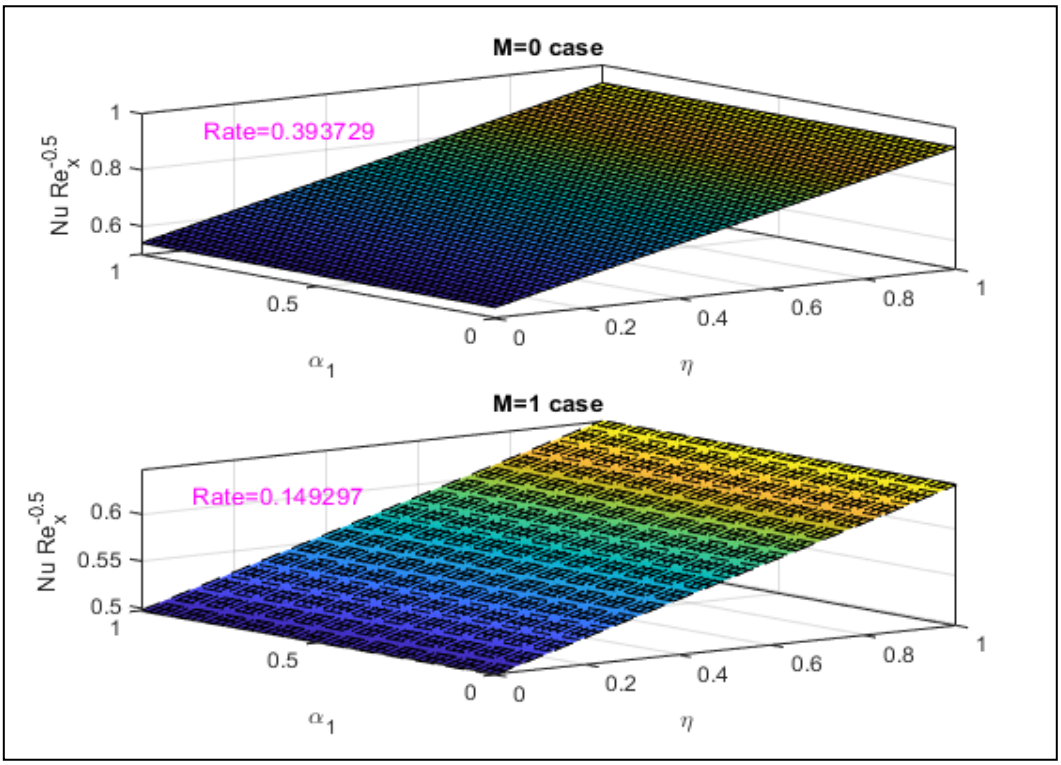

Figure 18. Surface plot of Nusselt number on α_1.

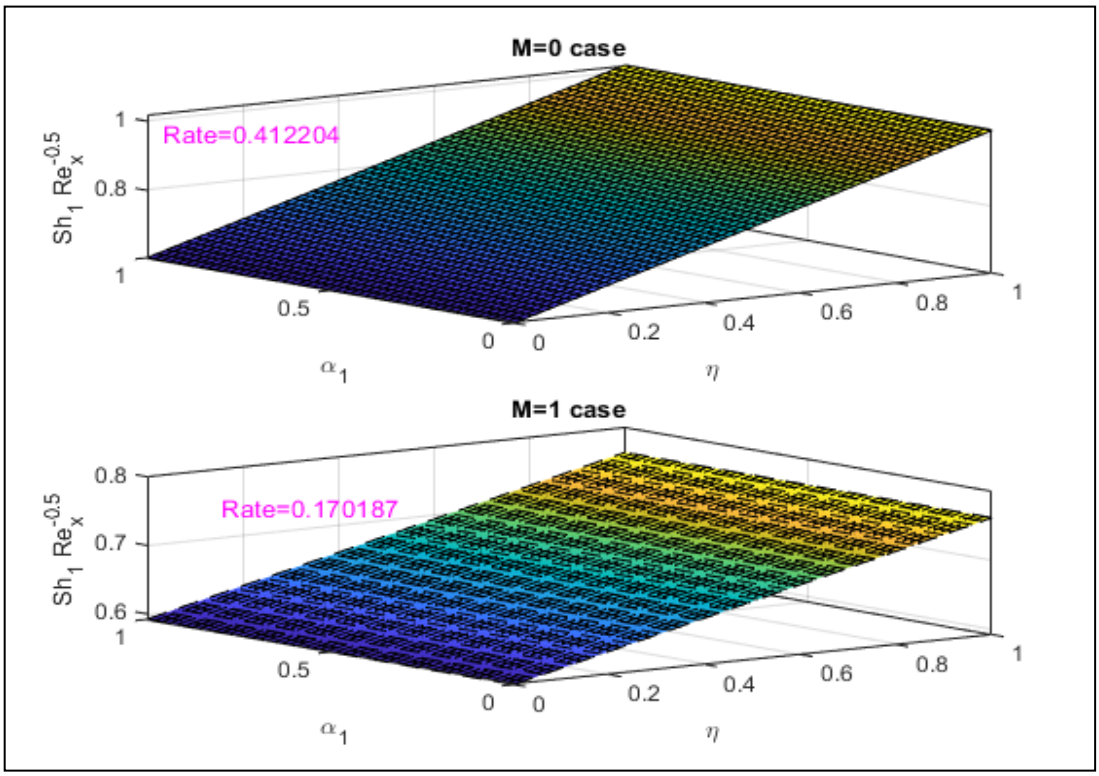

Figure 19. Surface plot of Salt 1 Sherwood number on α_1.

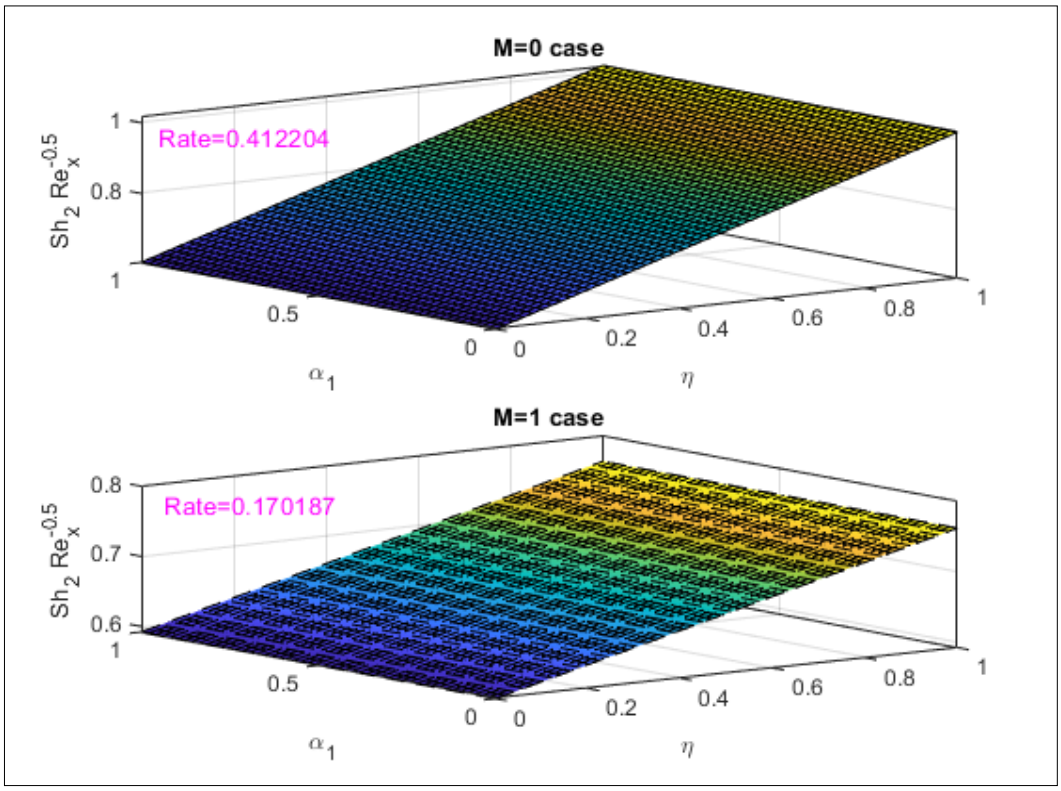

Figure 20. Surface plot of Salt 2 Sherwood number on α_1.

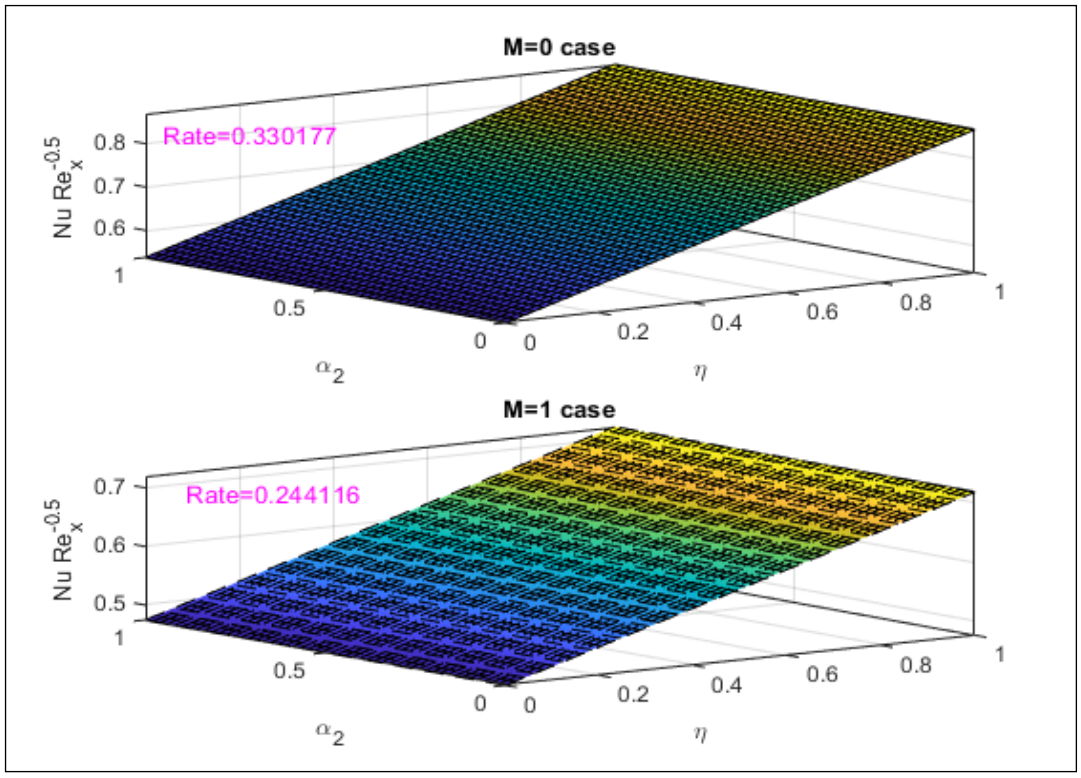

Figure 21. Surface plot of Nusselt number on α_1.

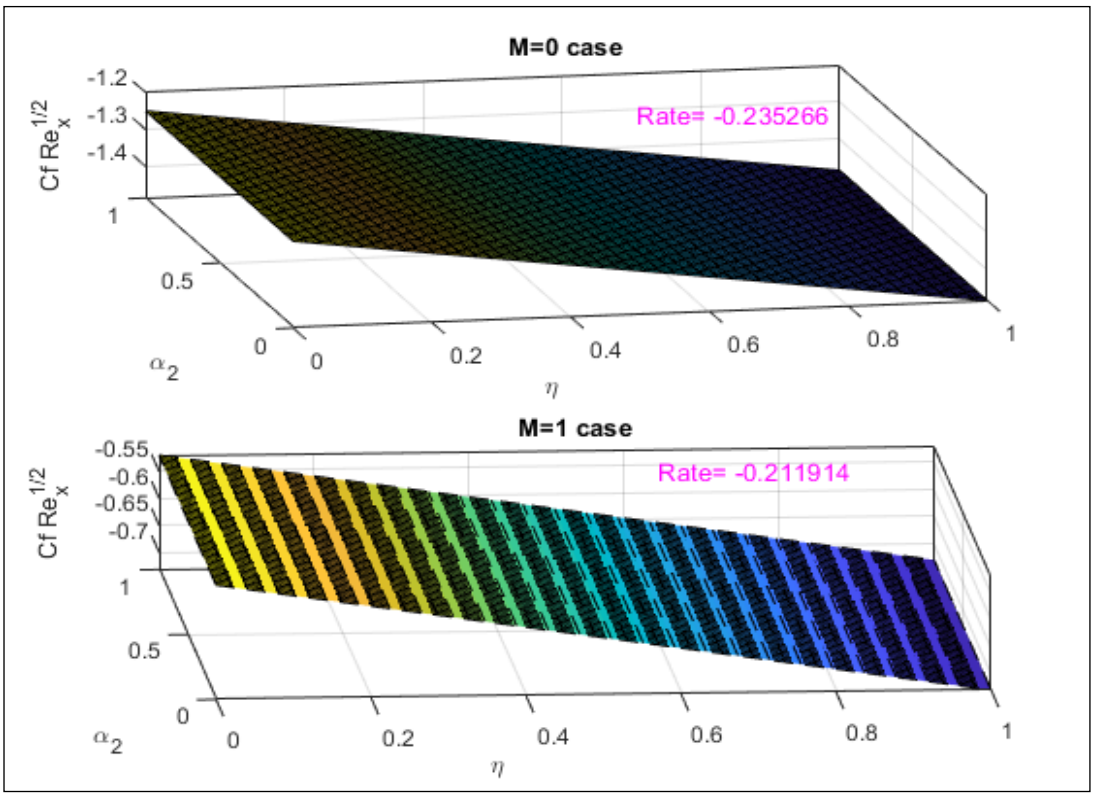

Figure 22. Surface plot of Skin friction on α_2.

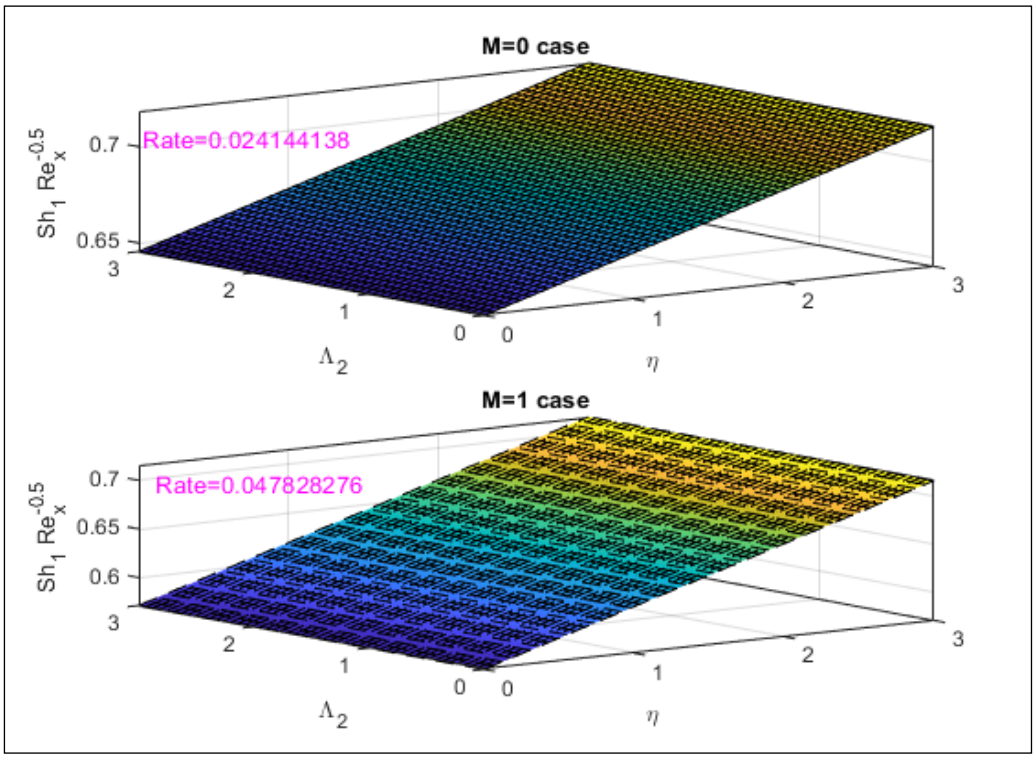

Figure 23. Surface plot of Salt 1 Sherwood number on Λ_2.

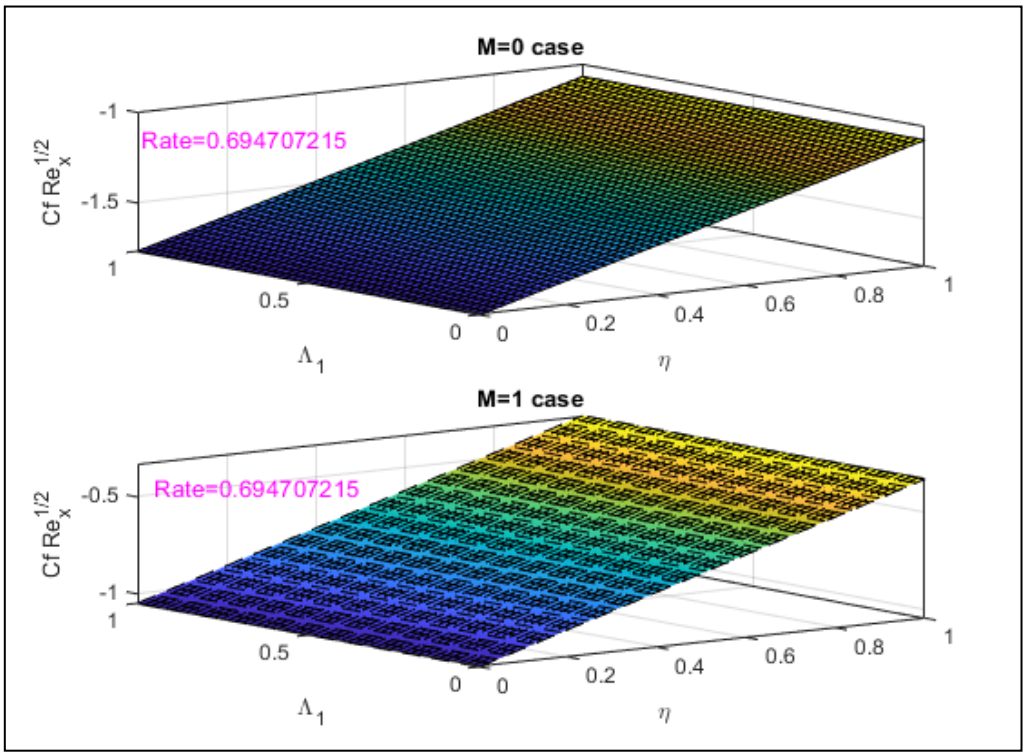

Figure 24. Surface plot of skin friction coefficient on Λ_1.

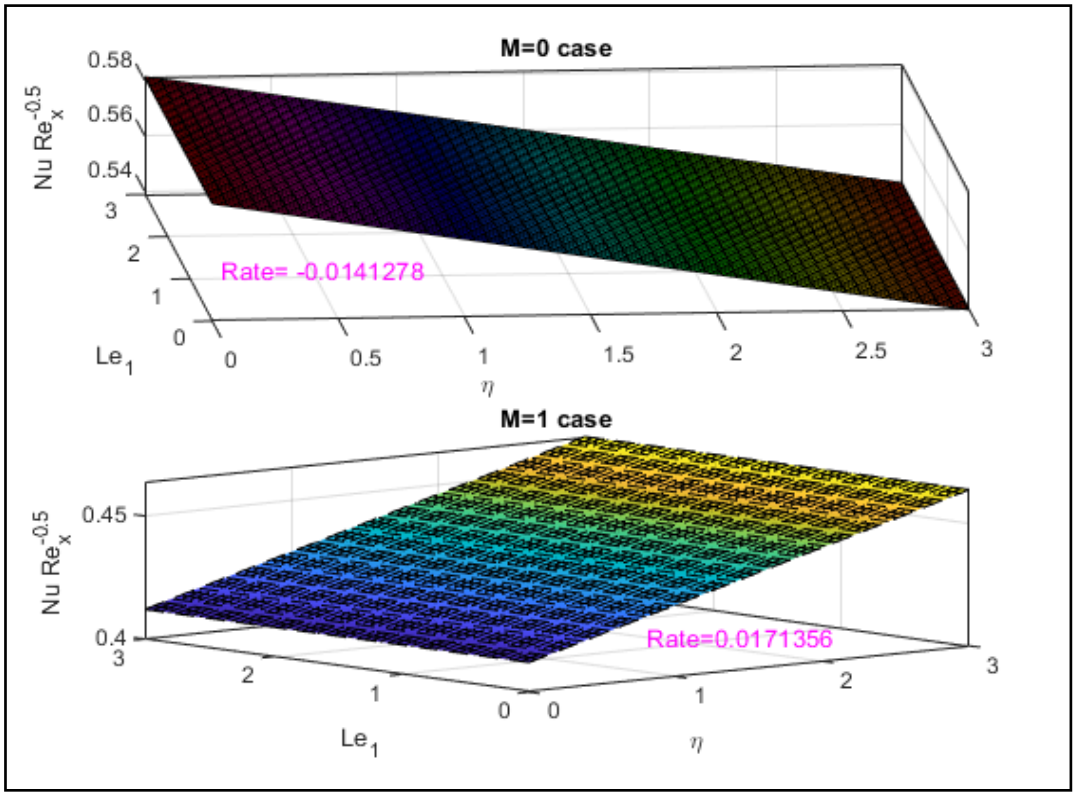

Figure 25. Surface plot of Nusselt number on Le_1.

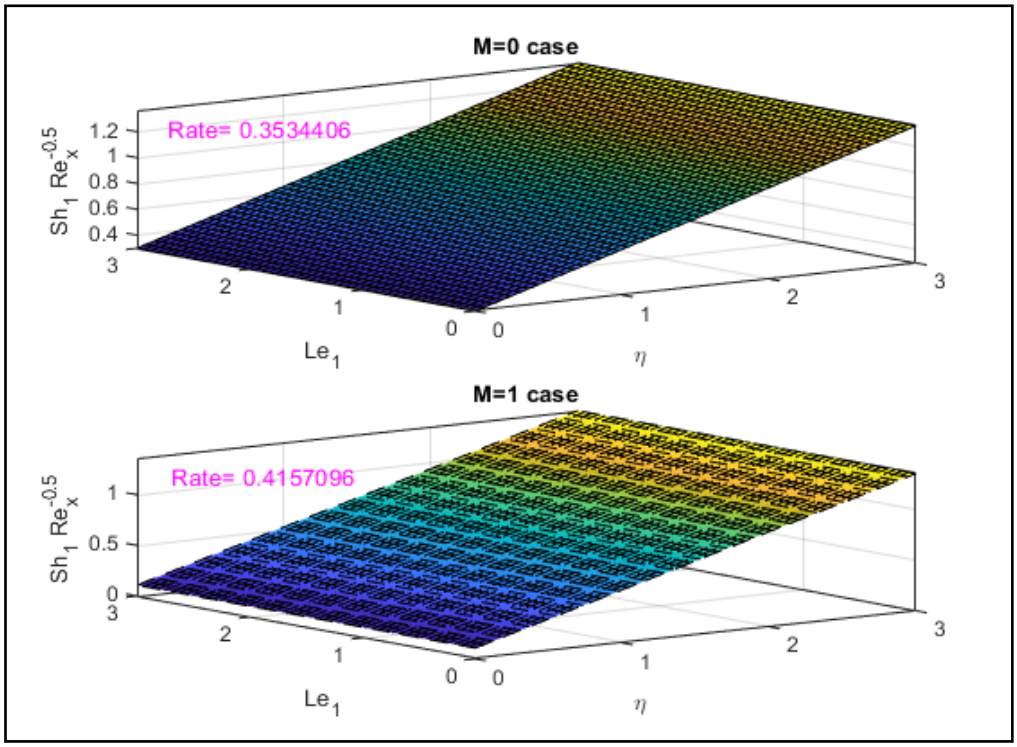

Figure 26. Surface plot of Salt 1 Sherwood number on Le_1.

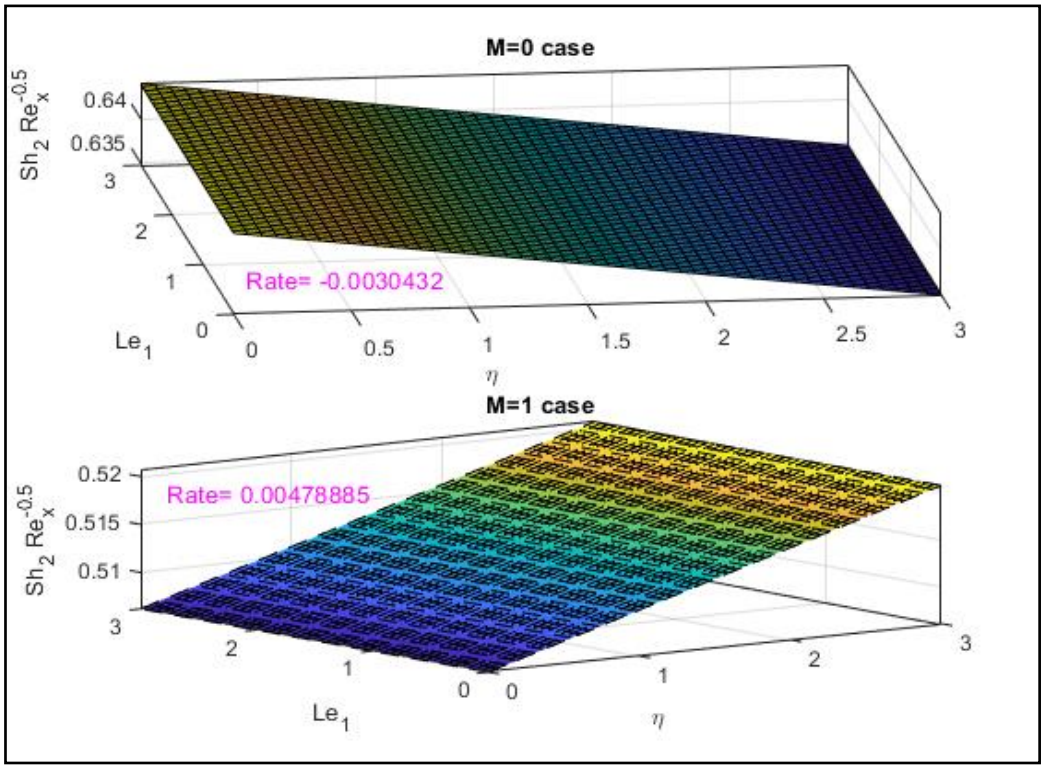

Figure 27. Surface plot of Salt 2 Sherwood number on Le_1.

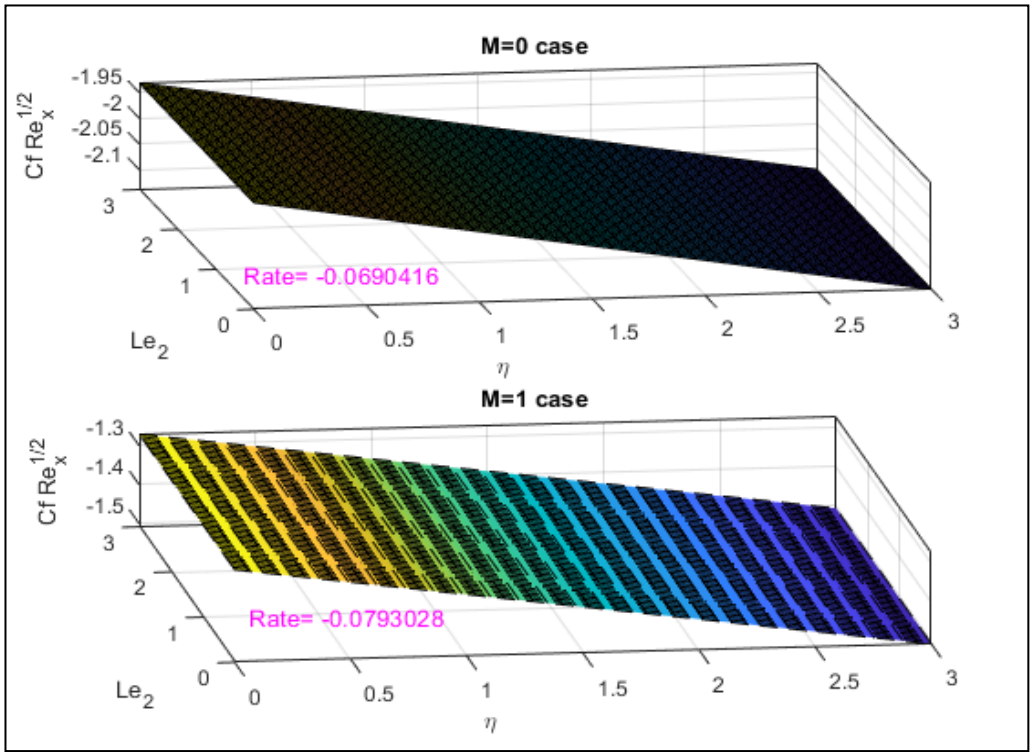

Figure 28. Surface plot of skin friction coefficient on Le_2.

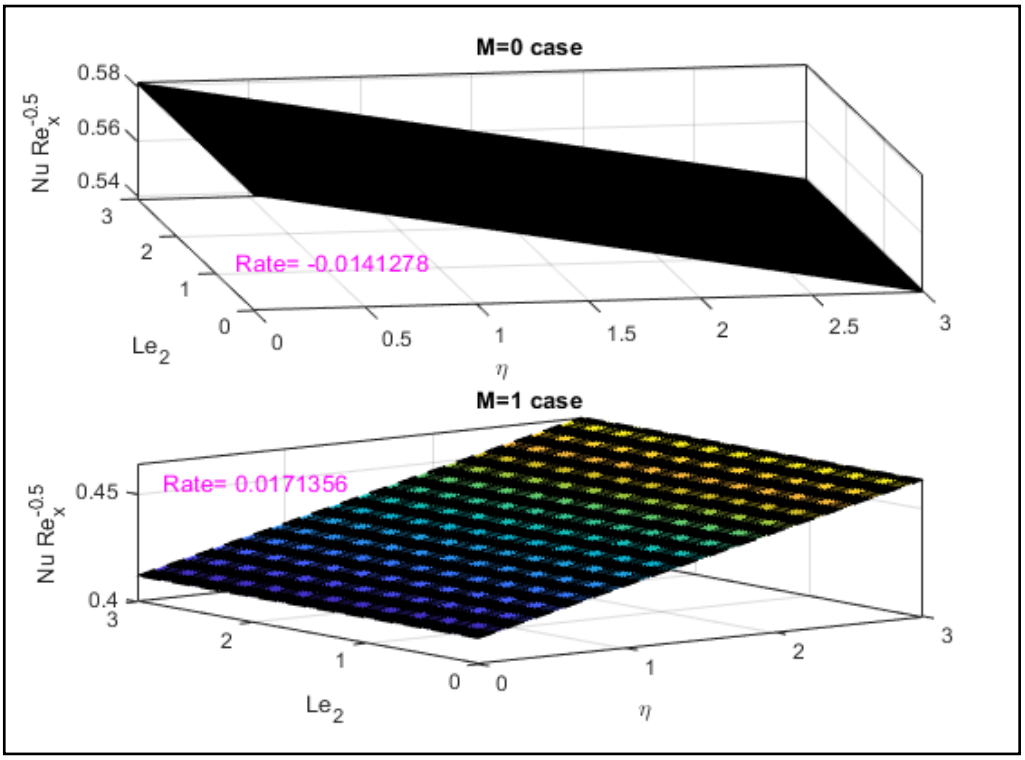

Figure 29. Surface plot of Nusselt number on Le_2.

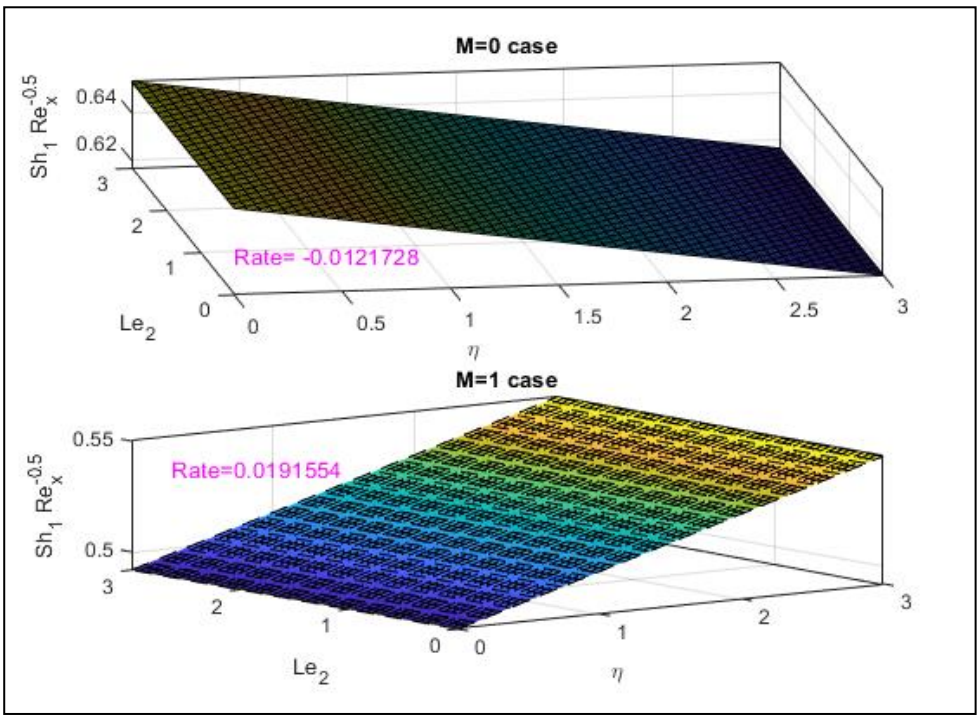

Figure 30. Surface plot of Salt 1 Sherwood number on Le_2.

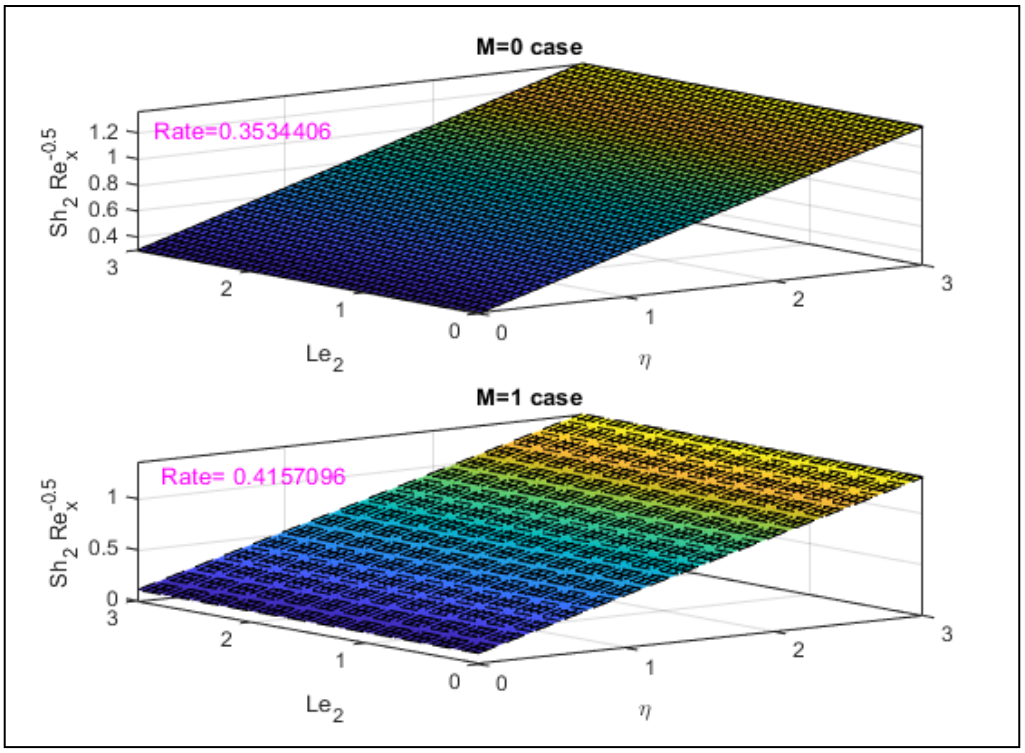

Figure 31. Surface plot of Salt 2 Sherwood number on Le_2.

5. Concluding remarks

A theoretical study has been conducted for laminar incompressible triple diffusive boundary layer flow in the presence and absence of a hydromagnetic fluid. Momentum and thermal slip effects have been incorporated into model. The transformed boundary layer equations for heat and momentum conservation have been solved by using Lie group transformation analysis. The present investigation has shown the following:

1. The momentum slip parameter α_1 improve the Nusselt number and Salt 1 and 2 Sherwood number in the presence and absence of a magnetic field.
2. The thermal slip parameter increases, less heat is transformed from the surface to the fluid and consequently the temperature decreases.
3. The momentum slip parameter reduces the skin friction coefficient for $M = 0$, but increases in the case of $M = 1$.
4. The Lewis number Le_1 enhances the Salt 1 Sherwood number for $M = 0$ and $M = 1$. The opposite behavior can be observed for the Salt 2 Sherwood number.
5. The thermal slip parameter α_2 enhances the Nusselt number in both the presence and absence of the magnetic field parameter.
6. The thermal and concentration buoyancy ratio parameters are upsurge the friction factor, Nusselt number and Salts 1 and 2 Sherwood numbers in both cases of magnetic field the parameter $M = 0$ and $M = 1$.
7. With the increase of the velocity and temperature, Salt 1 and 2 concentration distributions decreased because molecular forces dominate the thermal buoyancy forces.

Conflict of interest

The authors declare that they have no competing interests.

References

1. S. Lie, Sophus 1884 Differential Invariants Paper (Translation by M. Acherman, Comments by R. Hermann), Math. Sci. Press, Brookline, Mass., 1976.
2. L. V. Ovsiannikov, Group analysis of differential equations, Academic Press, New York, 1982. https://doi.org/10.1016/B978-0-12-531680-4.50012-5
3. M. M. Bhatti, S. Jun, C. M. Khalique, A. Shahid, L. Fasheng, M. S. Mohamed, Lie group analysis and robust computational approach to examine mass transport process using Jeffrey fluid model, *Appl. Math. Comput.*, **421** (2022), 126936. https://doi.org/10.1016/j.amc.2022.126936
4. H. sümer, Y. aksoy, Similarity Solutions of a non-Newtonian Fluid's Momentum and Thermal Boundary Layers: Cross Fluid Model, Afyon Kocatepe Üniversitesi Fen Ve Mühendislik Bilimleri Dergisi, **22** (2022), 222–239. https://doi:10.35414/akufemubid.1028006
5. N. A. Shah, A. Wakif, E. R. El-Zahar, S. Ahmad, S. J Yook, Numerical simulation of a thermally enhanced EMHD flow of a heterogeneous micropolar mixture comprising (60%)-ethylene glycol (EG), (40%)-water (W), and copper oxide nanomaterials (CuO), *Case Stud. Therm. Eng.*, **35** (2022), 102046. https://doi.org/10.1016/j.csite.2022.102046

6. K. U. Rehman, W. Shatanawi, K. Abodayeh, T. A. M. Shatnawi, A group theoretic analysis of mutual interactions of heat and mass transfer in a thermally slip Semi-Infinite domain, *Appl. Sci.*, **12** (2022). https://doi.org/10.3390/app12042000
7. V. Nagendramma, P. Durgaprasad, N. Sivakumar, B. M. Rao, C. S. Raju, N. A. Shah, et al., Dynamics of triple diffusive free convective MHD fluid flow: Lie group transformation, *Mathematics*, **10** (2022), 2456. https://doi.org/10.3390/math10142456
8. M. J. Babu, Y. S. Rao, A. S. Kumar, C. S. K. Raju, S. A. Shehzad, T. Ambreen, et al., Squeezed flow of polyethylene glycol and water based hybrid nanofluid over a magnetized sensor surface: A statistical approach, *Int. Commun. Heat Mass Transf.*, **135** (2022), 106136. https://doi.org/10.1016/j.icheatmasstransfer.2022.106136.
9. C. S. K. Raju, N. A. Ahammad, K. Sajjan, N. A. Shah, S. J. Yook, M. D. Kumar, Nonlinear movements of axisymmetric ternary hybrid nanofluids in a thermally radiated expanding or contracting permeable Darcy Walls with different shapes and densities: Simple linear regression, *Int. Comm. Heat Mass*, **135** (2022), 106110. https://doi.org/10.1016/j.icheatmasstransfer.2022.106110
10. P. Rana, M. J. Uddin, Y. Gupta, A. I. M. Ismail, Two-component modeling for non-Newtonian nanofluid slip flow and heat transfer over sheet: Lie group approach, *Appl. Math. Mech.*, **37** (2016), 1325–1340. https://doi.org/10.1007/s10483-016-2140-9
11. C. H. Amanulla, N. Nagendra, M. S. N. Reddy, Numerical study of thermal and momentum slip effects on MHD Williamson nanofluid from an isothermal sphere, *J. Nanofluids*, **6** (2017), 1111–1126. https://doi.org/10.1166/jon.2017.1405
12. X. Zhang, Y. Yang, T. Li, Y. Zhang, H. Wang, H. Fujita, CMC: A consensus multi-view clustering model for predicting Alzheimer's disease progression, *Comput. Meth. Prog. Bio.*, **199** (2021), 105895. https://doi.org/10.1016/j.cmpb.2020.105895
13. S. Batool, G. Rasool, N. Alshammari, I. Khan, H. Kaneez, N. Hamadneh, Numerical analysis of heat and mass transfer in micropolar nanofluids flow through lid driven cavity: Finite volume approach, *Case Stud. Therm. Eng.*, **37** (2022), 102233. https://doi.org/10.1016/j.csite.2022.102233
14. A. Maneengam, H. Laidoudi, A. Abderrahmane, G. Rasool, K. Guedri, W. Weera, et al., Entropy generation in 2D Lid-Driven porous container with the presence of obstacles of different shapes and under the influences of Buoyancy and Lorentz Forces, *Nanomaterials*, **12** (2022), 2206. https://doi.org/10.3390/nano12132206
15. M. S. Bhutta, T. Xuebang, S. Akram, C. Yidong, X. Ren, M. Fasehullah, et al., Development of novel hybrid 2D-3D graphene oxide diamond micro composite polyimide films to ameliorate electrical & thermal conduction, *J. Ind. Eng. Chem.*, **114** (2022), 108–114. https://doi.org/10.1016/j.jiec.2022.06.036
16. G. Rasool, N. A. Shah, E. R. El-Zahar, A. Wakif, Numerical investigation of EMHD nanofluid flows over a convectively heated riga pattern positioned horizontally in a Darcy-Forchheimer porous medium: Application of passive control strategy and generalized transfer laws, Waves and Random Complex Media, 2022. https://doi.org/10.1080/17455030.2022.2074571.
17. G. Rasool, A. M. Saeed, I. L. Animasaun, A. Abderrahmane, K. Guedri, et al., Darcy-Forchheimer flow of water conveying multi-walled carbon nanoparticles through a vertical Cleveland Z-Staggered Cavity Subject to entropy generation, *Micromachines*, **13** (2022), 744. https://doi.org/10.3390/mi13050744

18. U. Arif, M. A. Memon, R. S. Saif, A. S. EI-Shafay, M. Nawaz, T. Muhammed, Triple diffusion with heat transfer under different effects on magnetized hyperbolic tangent nanofluid flow, *J. P. Mech. Eng.*, **3** (2022), https://doi.org/10.1177/09544089221079139.
19. P. M. Patil, S. Benawadi, B. Shanker, Influence of mixed convection nanofluid flow over a rotating sphere in the presence of diffusion of liquid hydrogen and ammonia, *Math. Comp. Simulat.*, **194** (2022), 764–781. https://doi.org/10.10.1016/j.matcom.2021.12.022
20. M. Nawaz, M. Awais, Triple diffusion of species in fluid regime using tangent hyperbolic rheology, *J. Therm. Anal. Calorim.*, **146** (2021), 775–785, https://doi.org/10.1007/s10973-020-10026-0.
21. A. Manjappa, G. B. Jayanna, P. B. Chandrappa, Triple diffusive flow of Casson nanofluid with buoyancy forces and nonlinear thermal radiation over a horizontal plate, *Heat Transfer*, **47** (2018), 957–973. https://doi.org/10.1002/htj.21360
22. P. M. Patil, A. Shashikant, E. Momoniat, C. Harley, Numerical simulation of unsteady triple diffusive mixed convection in NaCl-water and Sucrose-water solutions, *Int. J. Heat Mass Transf.*, **126** (2018), 147–155. https://doi.org/10.1016/j.ijheatmasstransfer.2018.05.166
23. P. M. Patil, A. Shashikant, P. S. Hiremath, Influence of liquid hydrogen and nitrogen on MHD triple diffusive mixed convection nanoliquid flow in presence of surface roughness, *Int. J. Hydrog. Energ.*, **43** (2018), 20101–20117. https://doi.org/10.1016/j.ijhydene.2018.09.033
24. P. Y. Xiong, M. Nazeer, F. Hussain, M. I. Khan, A. Saleem, S. Qayyum, et al., Two-phase flow of couple stress fluid thermally effected slip boundary conditions: Numerical analysis with variable liquids properties, *Alex. Eng. J.*, **61** (2022), 3821–3830. https://doi.org/10.1016/j.aej.2021.09.012.
25. O. A. Bég, T. Bég, W. A. Khan, M. J. Uddin, Multiple slip effects on nanofluid dissipative flow in a converging/diverging channel: A numerical study, *Heat Transfer*, **51** (2022), 1040–1061. https://doi.org/10.1002/htj.22341.
26. L. Su, B. He, G. Wang, R. Xiao, W. Yu, Simultaneously developing flow and heat transfer in circular and parallel-plates microchannels with velocity slip and temperature jump, International *J. Therm. Sci.*, **177** (2022), 107590. https://doi.org/10.1016/j.ijthermalsci.2022.107590
27. K. N. Sneha, U. S. Mahabaleshwar, Y. Sheikhnejad, Heat and Mass Transfer of Walters' Liquid B Flow Over A Porous Stretching/Shrinking Plate with Mass Transpiration and Slip, Transport in Porous Media, (2022). https://doi.org/10.1007/s11242-022-01758-8
28. A. Sabu, A. Wakif, S. Areekara, A. Mathew, N. A. Shah, Significance of nanoparticles' shape and thermo-hydrodynamic slip constraints on mhd alumina-water nanoliquid flows over a rotating heated disk: The passive control approach, *Int. Commun. Heat Mass Transf.*, **129** (2021), 105711. https://doi.org/10.1016/j.icheatmasstransfer.2021.105711
29. O. K. Koriko, K. S. Adegbie, N. A. Shah, I. L. Animasaun, M. A. Olotu, Numerical solutions of the partial differential equations for investigating the significance of partial slip due to lateral velocity and viscous dissipation: The case of blood-gold Carreau nanofluid and dusty fluid, *Numer. Meth. Part. D. E.*, (2021), 1–29. https://doi.org/ 10.1002/num.22754
30. E. Seid, E. Hailen, T. Walelign, Multiple slip, Soret and Dufour effects in fluid flow near a vertical stretching sheet in the presence of magnetic nanoparticles, *Int. J. Therm.*, **13** (2022), 100136. https://doi.org/10.1016/j.ijft.2022.100136
31. M. Turkyilmazoglu, Velocity Slip and Entropy Generation Phenomena in Thermal Transport Through Metallic Porous Channel, *J. Non-Equil. Thermody.*, **45** (2020). https://doi.org/10.1515/jnet-2019-0097

32. F. L. Paiva, A. R. Secchi, V. Calado, J. Maia, S. Khani, Slip and momentum transfer mechanisms mediated by Janus rods at polymer interfaces, *Soft Matter*, **16** (2020), 6662–6672. https://doi.org/10.1039/D0SM00858C
33. A. Majeed, F. M. Noori, A. Zeeshan, T. Mahmood, S. U. Rehman, I. Khan, Analysis of activation energy in magnetohydrodynamic flow with chemical reaction and second order momentum slip model, *Case Stud. Therm. Eng.*, **12** (2018), 765–773. https://doi.org/10.1016/j.csite.2018.10.007
34. A. Majeed, A. Zeeshan, F. M. Noori, Numerical study of Darcy-Forchheimer model with activation energy subject to chemically reactive species and momentum slip of order two, *AIP Adv.*, **9** (2019), 045035. https://doi.org/10.1063/1.5095546
35. M. Ferdows, M. J. Uddin, A. A. Afify, Scaling group transformation for MHD boundary layer free convective heat and mass transfer flow past a convectively heated nonlinear radiating stretching sheet, *Int. J. Heat Mass Transf.*, **56** (2013), 181–187.

AIMS Press